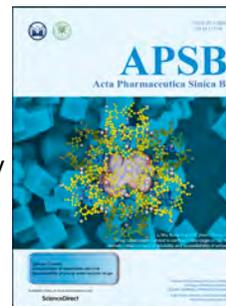# Journal Pre-proof

The E3 ubiquitin ligase NEDD4-1 protects against acetaminophen-induced liver injury by targeting VDAC1 for degradation

Yiwei Zhu, Lin Lei, Xinghui Wang, Linfang Chen, Wei Li, Jinxia Li, Chenchen Zhao, Xiliang Du, Yuxiang Song, Wenwen Gao, Guowen Liu, Xinwei Li

Please cite this article as: Zhu Y, Lei L, Wang X, Chen L, Li W, Li J, Zhao C, Du X, Song Y, Gao W, Liu G, Li X, The E3 ubiquitin ligase NEDD4-1 protects against acetaminophen-induced liver injury by targeting VDAC1 for degradation, *Acta Pharmaceutica Sinica B*, https://doi.org/10.1016/j.apsb.2023.01.019.

This is a PDF file of an article that has undergone enhancements after acceptance, such as the addition of a cover page and metadata, and formatting for readability, but it is not yet the definitive version of record. This version will undergo additional copyediting, typesetting and review before it is published in its final form, but we are providing this version to give early visibility of the article. Please note that, during the production process, errors may be discovered which could affect the content, and all legal disclaimers that apply to the journal pertain.

Original article

The E3 ubiquitin ligase NEDD4-1 protects against acetaminophen-induced liver injury by targeting VDAC1 for degradation

Yiwei Zhu[†], Lin Lei[†], Xinghui Wang, Linfang Chen, Wei Li, Jinxia Li, Chenchen Zhao, Xiliang Du, Yuxiang Song, Wenwen Gao, Guowen Liu[*], Xinwei Li[*]

State Key Laboratory for Zoonotic Diseases, Key Laboratory of Zoonosis Research, Ministry of Education, College of Veterinary Medicine, Jilin University, Changchun 130062, China

[*]Corresponding authors. Tel.: +86 0431 87836160; fax: +86 0431 87836156.

E-mail addresses: liuguowen2008@163.com (Guowen Liu); lixinwei100@jlu.edu.cn (Xinwei Li).

[†]These authors contributed equally to this work.

Running title: NEDD4-1 protects against AILI by targeting VDAC1 for degradation

Graphical abstract
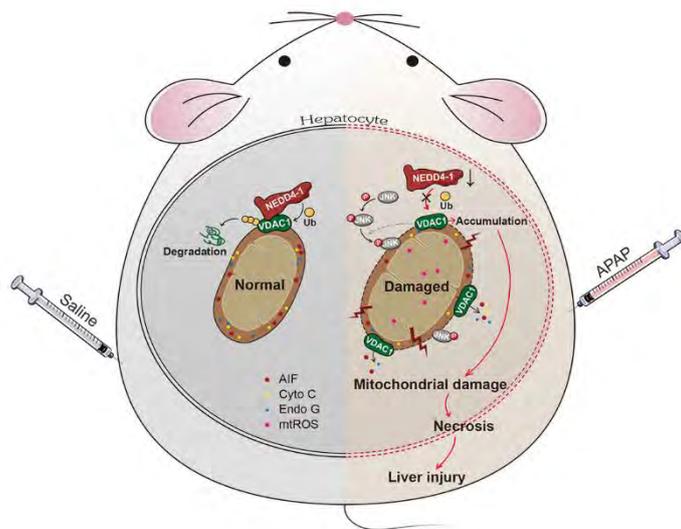
This study indicates that NEDD4-1 is a suppressor of APAP-induced liver injury and functions by regulating the degradation of voltage-dependent anion channel 1.

Journal Pre-proof

Original article

The E3 ubiquitin ligase NEDD4-1 protects against acetaminophen-induced liver injury by targeting VDAC1 for degradation

Yiwei Zhu[†], Lin Lei[†], Xinghui Wang, Linfang Chen, Wei Li, Jinxia Li, Chenchen Zhao, Xiliang Du, Yuxiang Song, Wenwen Gao, Guowen Liu[*], Xinwei Li[*]

State Key Laboratory for Zoonotic Diseases, Key Laboratory of Zoonosis Research, Ministry of Education, College of Veterinary Medicine, Jilin University, Changchun 130062, China

[*]Corresponding authors. Tel.: +86 431 87836160; fax: +86 431 87836156.

E-mail addresses: liuguowen2008@163.com (Guowen Liu); lixinwei100@jlu.edu.cn (Xinwei Li).

[†]These authors contributed equally to this work.

Running title: NEDD4-1 protects against AILI by targeting VDAC1 for degradation

Abstract Acetaminophen (APAP) overdose is a major cause of liver injury. Neural precursor cell expressed developmentally downregulated 4-1 (NEDD4-1) is an E3 ubiquitin ligase that has been implicated in the pathogenesis of numerous liver diseases; however, its role in APAP-induced liver injury (AILI) is unclear. Thus, this study aimed to investigate the role of NEDD4-1 in the pathogenesis of AILI. We found that NEDD4-1 was dramatically downregulated in response to APAP treatment in mouse livers and isolated mouse hepatocytes. Hepatocyte-specific NEDD4-1 knockout exacerbated APAP-induced mitochondrial damage and the resultant hepatocyte necrosis and liver injury, while hepatocyte-specific NEDD4-1 overexpression mitigated these pathological events both *in vivo* and *in vitro*. Additionally, hepatocyte NEDD4-1 deficiency led to marked accumulation of voltage-dependent anion channel 1 (VDAC1) and increased VDAC1 oligomerization. Furthermore, VDAC1 knockdown alleviated AILI and weakened the exacerbation of AILI caused by hepatocyte NEDD4-1 deficiency. Mechanistically, NEDD4-1 was found to interact with the PPTY motif of VDAC1 through its WW domain and regulate K48-linked ubiquitination and degradation of VDAC1. Our present study indicates that NEDD4-1 is a suppressor of AILI and functions by regulating the degradation of VDAC1.

KEY WORDS Acetaminophen; NEDD4-1; VDAC1; Liver injury; Hepatotoxicity;

Necrosis; Mitochondrial damage; Ubiquitination

1. Introduction

Acetaminophen (APAP), also called paracetamol, is a widely used analgesic that is safe at therapeutic doses[1-3]. However, APAP induces various degrees of liver damage when ingested at supratherapeutic doses or misused by at-risk individuals, and APAP overdose is currently the most frequent cause of drug-induced acute liver injury in many countries[2,4,5]. APAP-induced liver injury (AILI) accounts for 39% and 57% of acute liver failure cases in the USA and UK, respectively[4,5].

The hepatotoxicity of APAP stems from its reactive metabolite, *N*-acetyl-*p*-benzoquinone imine (NAPQI)[6,7]. When APAP overdose occurs, excessive NAPQI generated by cytochrome p450 enzymes (CYPs, mainly CYP2E1) rapidly depletes glutathione (GSH) and binds to intracellular proteins, especially mitochondrial proteins[6-8], resulting in mitochondrial damage, adenosine triphosphate (ATP) depletion, nuclear DNA damage and, ultimately, necrotic cell death in hepatocytes[9-11]. These pathological events are mutually promoted and thus lead to severe or even irreversible liver failure. Therefore, strategies for AILI therapy should target a key factor that is involved in prominent pathogenic pathways to ultimately inhibit multiple pathological features.

Ubiquitination is a posttranslational modification process that is accomplished *via* a sequential enzymatic catalytic cascade[12-14] and requires an E3 ubiquitin ligase, which is the primary determinant of substrate specificity for ubiquitination[15-17]. By regulating intracellular protein fate, ubiquitination governs practically all aspects of cellular function and modulates cellular physiological and pathological processes[12-14]. Hence, it is constructive to discover key ubiquitination-related modulators implicated in the pathological mechanisms of AILI. Neural precursor cell expressed developmentally downregulated 4-1 (NEDD4-1), a member of the homologous to the E6-AP COOH terminus (HECT) E3 ubiquitin ligase family, is characterized by a C-terminal HECT domain, four WW repeats and an N-terminal C2 domain[18]. Studies have shown that NEDD4-1 targets many ubiquitination substrates *via* interactions with its WW domains and regulates diverse cellular physiological processes, including endocytosis, inflammasome activation, cell growth and proliferation, and autophagy[19]. Notably, aberrant expression of NEDD4-1 is associated with multiple human diseases[20-22], such

as endotoxic shock[23], liver regeneration disorder[24], ischemia/reperfusion injury[21,25,26], and cancer[22,27]. However, to the best of our knowledge, no prior study has reported the role of NEDD4-1 in AILI.

In the current study, we reveal that NEDD4-1 is a key suppressor of APAP-induced mitochondrial damage, necrosis and liver injury. Mechanistically, NEDD4-1 directly interacts with voltage-dependent anion channel 1 (VDAC1) and mediates its K48-linked polyubiquitination and subsequent degradation, thereby protecting against APAP-induced mitochondrial damage, necrosis and liver injury.

2. Materials and methods

2.1. Animals and treatment

Experimental animal protocols were approved by the Ethics Committee for Animal Care and Use of Jilin University (permit number: SY202008007; Changchun, China). The animals were treated humanely according to *Laboratory animal-the guidelines for ethical review of animal welfare* (GB/T 35892-2018, China). Wild-type (WT) C57BL/6N mice were purchased from Cyagen Biosciences (Suzhou, China). Mice with the floxed *Nedd4-1* alleles (Flox; on a C57BL/6N background) were also purchased from Cyagen Biosciences. Hepatocyte-specific *Nedd4-1* knockout (HepKO; on a C57BL/6N background) mice were generated by mating Flox mice with albumin-Cre mice (Cyagen Biosciences). Although it is now increasingly recognized that crossing Flox mice with albumin-Cre mice will not generate pure hepatocyte specific knockout mice since albumin is expressed in bipotent fetal liver progenitor cells that give rise to both hepatocytes and biliary cells[28], albumin-Cre mice is still widely used and acceptable for generating hepatocyte specific knockout mice today[29-31]. All experiments described in this report used male mice aged 4–8 weeks. Mice were housed in a temperature (23 ± 2 °C) and humidity ($40 \pm 5\%$) controlled specific pathogen-free facility with a 12 h/12 h dark/light photocycle. Food and water were provided *ad libitum*.

For modeling AILI mouse models, mice were fasted overnight to reduce hepatic GSH levels before APAP injection. APAP (IA0030; Solarbio, Beijing, China) was dissolved in warm saline (0.9% NaCl; 55 °C), cooled to 37 °C, and injected intraperitoneally at a dose of 300 or 600 mg/kg. Animals were sacrificed 6, 12, or 24 h after APAP administration. Liver and serum samples at each indicated time point were collected for further experiments.

2.2. Analysis of serum parameters

Serum alanine aminotransferase (ALT), aspartate aminotransferase (AST), lactate dehydrogenase (LDH) activities, and high mobility group box 1 (HMGB1) concentration were measured using the ALT activity assay kit (MAK052; Sigma–Aldrich, St. Louis, MO, USA), AST activity assay kit (MAK055; Sigma–Aldrich), LDH activity assay kit (MAK066; Sigma–Aldrich), and mouse HMGB1 ELISA kit (NBP2-62767; Novus Biologicals, Littleton, CO, USA) according to the manufacturer's protocols, respectively.

2.3. Hematoxylin and eosin (H&E) and immunohistochemical (IHC) staining

H&E and IHC staining were performed in paraffin-embedded liver sections. Briefly, liver samples were fixed in 4% paraformaldehyde overnight, dehydrated, cleared, and embedded in paraffin. The waxes were sectioned serially at 3–5 μm thickness. After deparaffinization and rehydration, standard H&E staining was carried out to visualize the pattern in necrotic areas of the liver. The VDAC1 expression profiles in mice liver samples were determined by incubating the liver sections with anti-VDAC1 primary antibodies. Histological features were observed and captured under a light microscope (Olympus Corporation, Tokyo, Japan). The details of antibodies are listed in Supporting Information Table S1.

2.4. Protein extraction and Western blotting

Total protein was extracted from liver tissue or cells, and prepared for Western blotting according to manufacturer's instructions (P0013K; Beyotime Institute of Biotechnology, Shanghai, China). Mitochondrial and cytosolic fractions used for Western blotting were isolated from fresh liver tissue or hepatocytes using a mitochondria isolation kit (MP-007; Invent Biotechnologies, Eden Prairie, MN, USA) according to manufacturer's instructions. Protein abundance of each molecular was determined by Western blotting as previously described[32]. The details of antibodies are listed in Table S1.

2.5. RNA extraction and quantitative real-time polymerase chain reaction

Protocol for quantitative real-time polymerase chain reaction was the same as described

previously[32,33]. Briefly, total RNA was extracted using RNAiso Plus (D9108, TaKaRa Biotechnology, Dalian, China) according to manufacturer's instructions. Complementary DNA was reverse-transcribed from 1 μg total RNA using a reverse transcription kit (RR047A, TaKaRa Biotechnology). Relative mRNA expression of target genes was detected using the TB Green Premix Ex Taq II (RR82LR, TaKaRa Biotechnology) on the 7500 Real-Time PCR System (Applied Biosystems, Bedford, MA, USA). The relative expression of target genes was normalized to reference gene (*Actb*) using $2^{-\Delta\Delta CT}$ method[34]. Primer sequences are listed in Supporting Information Table S2.

2.6. Cell isolation, culture, and treatment

Mouse primary hepatocytes were isolated from 6- to 8-week-old male mice (C57BL/6N background) as previously described[35,36], with modification. Briefly, mice were anesthetized and perfused *in situ* with D-HBSS (PB180322; Procell Life Science & Technology, Wuhan, China) containing 5 mmol/L EDTA and then HBSS (PB130824; Procell Life Science & Technology) containing 0.5 mg/mL collagenase type IV (17104019; Gibco, Grand Island, NY, USA) *via* the portal vein. The cell suspension was filtered through a 70-μm cell strainer (431751; Corning, NY, USA) and centrifuged at $50 \times g$ for 5 min at 4 °C. After that, the cell pellets were resuspended and mounted over a cushion of 25% Percoll (17089101; Cytiva Sweden AB, Uppsala, Sweden) to eliminate non-parenchymal cells. The obtained hepatocytes were washed with DMEM (SH30021.01; HyClone, Logan, UT, USA) and then cultured with William's E medium (PM151213; Procell Life Science & Technology) containing 10% fetal bovine serum (FBS; FB15015; Clark Bioscience, Richmond, VA, USA) in a 37 °C incubator with 5% CO_2 and humidified atmosphere. Endothelial cells, cholangiocytes and stromal cells were isolated based on bilio-vascular tree isolation procedure as previously described[37]. *In situ* perfusion of the liver was performed as described above. The digested liver was acquired and placed in pre-chilled DMEM. Liver parenchyma was mechanically detached and discarded. The remaining bilio-vascular tree was minced and digested in DMEM containing 0.075 mg/mL collagenase P (11213865001; Roche, Indianapolis, IN, USA), 0.02 mg/mL DNase I (D8071; Solarbio, Beijing, China), 3% FBS, 1 mg/mL bovine serum albumin, 1% HEPES and 1% Penicillin–Streptomycin at 37 °C. The digested bilio-vascular fragments were collected on top of a 40-μm cell strainer

(352340; Corning) and digested in 0.05% Trypsin-EDTA containing 0.02 mg/mL DNase I at 37 °C. Endothelial cells and cholangiocytes were isolated through a magnetic selection method using CD31 microbeads (130-097-418; Miltenyi Biotec, San Diego, CA, USA) and EpCAM microbeads (130-105-958; Miltenyi Biotec), respectively. Enriched stromal cell fraction was collected after excluding endothelial cells and cholangiocytes. 293T cell lines were purchased from the Cell Bank of Type Cultural Collection of Chinese Academy of Sciences (Shanghai, China), and cultured in DMEM (SH40007.01; HyClone) supplemented with 10% FBS at a 37 °C incubator with 5% CO_2.

To detect the effect of APAP on NEDD4-1 *in vitro*, primary hepatocytes were treated with different concentrations (0, 5, 10, or 20 mmol/L) of APAP for 12 h, or 10 mmol/L APAP for different times (0, 3, 6, or 12 h). To mimic APAP-induced hepatotoxicity *in vitro*, primary hepatocytes were treated with 10 mmol/L APAP for 12 h. To overexpress NEDD4-1 or knockdown VDAC1 *in vitro*, hepatocytes were infected with adenovirus expressing mouse *Nedd4-1* gene sequence (Ad-NEDD4-1) or adenovirus expressing short hairpin RNA (shRNA) targeting mouse *Vdac1* gene (Ad-shVDAC1) at a multiplicity of infection of 50 for 36–48 h, respectively. To inhibit the lysosomal degradation pathway of proteins, hepatocytes were treated with lysosome inhibitor chloroquine (CQ; 50 μmol/L) for 6 h before harvest. To inhibit the proteasomal degradation pathway of proteins, hepatocytes were treated with proteasome inhibitor MG132 (10 μmol/L) for 10 h before harvest. To inhibit c-Jun N-terminal kinase (JNK) signaling, hepatocytes were pretreated with 20 μmol/L SP600125 2 h before APAP treatment. For coimmunoprecipitation assays, 293T cells were transfected with the indicated plasmids for 24–48 h using Lipofectamine 3000 (L3000015; Invitrogen, Carlsbad, CA, USA).

2.7. Immunofluorescence assay

For immunofluorescence, cells were fixed with 4% paraformaldehyde at room temperature for 15 min, washed twice with PBS, and then permeabilized with 0.1% Triton X-100 for 1 h. After washing with PBS twice, cells were incubated with primary antibodies diluted in PBS containing 5% bovine serum albumin overnight at 4 °C. Cells were then washed three times for 5 min with Tris-buffered saline–Tween 20, and incubated with corresponding fluorescent secondary antibodies. Subsequently, cells

6

were washed twice with Tris-buffered saline–Tween 20, and then stained with DAPI. Cells were observed by a laser scanning confocal microscopy (Olympus FluoView 1200; Olympus Corporation). Fluorescence line profile and co-localization analyses were performed with Fiji software[38]. The details of antibodies are listed in Table S1.

2.8. RNA sequencing (RNA-seq) and data processing

For the RNA-seq analysis, total RNA was extracted from liver samples of APAP-treated Flox or APAP-treated HepKO mice. Libraries were constructed from total RNA and paired-end sequencing was performed on an Illumina Novaseq 6000 (Illumina, San Diego, CA, USA). Raw sequencing data were quality-controlled with Cutadapt and FastQC program. Reads were matched to reference genome sequences (mm10/GRCm38) using HISAT2 (version 2.1.0). Fragment per kilobase of transcript per million mapped reads mapped value was estimated by StringTie (version 1.3.4d). Differential gene expression analysis was performed using DEseq2 (version 1.2.10) according to the following two criteria: (1) folding change ≥ 2 and (2) false discovery rate < 0.05. The hierarchical clustering analysis was performed to analyze global sample distribution profiles by constructing a clustering tree based on data from RNA-seq by R function hclust. Gene set enrichment analysis (GSEA) was performed using the R package ReactomePA (version 1.30.0) with default parameters. Gene sets with P values < 0.05 were considered statistically significant. RNA-seq data generated in this study have been deposited in the Gene Expression Omnibus public database under accession number GSE199353.

2.9. Measurement of viable and dead cells

Calcein-AM/propidium iodide (PI) double staining kit (40747ES76; Yeasen Biotechnology, Shanghai, China) was utilized for simultaneous fluorescence staining of viable and dead cells. This kit contains Calcein-AM and PI solutions, which stain viable and dead cells, respectively. After treatment as indicated in results, cells were stained according to manufacturer's instruction. Firstly, washing cells with 1× assay buffer three times to remove residual esterase activity. After that, cells were incubated with the working solution (2 µmol/L Calcein-AM and 4.5 µmol/L PI in 1× assay buffer) for 20 min at 37 °C, protected from light. Following incubation, cells were washed gently with 1× assay buffer three times, and then visualized by a laser scanning confocal

microscopy (Olympus FluoView 1200).

2.10. Adeno-associated virus 8 (AAV8) injection

The AAV8 delivery system was constructed by Vigene Bioscience (Jinan, China). For NEDD4-1 overexpression, mice were injected with AAV8-TBG (a genetic delivery system containing hepatocyte-specific promoter TBG and exhibiting high specificity and transfection efficiency in hepatocytes) carrying the full length mouse *Nedd4-1* gene sequence (AAV8-NEDD4-1). For *VDAC1* knockdown, mice were injected with AAV8 vectors bearing shRNA targeting mouse *Vdac1* gene (AAV8-shVDAC1). Mice were injected in the lateral tail vein with 200 µL of virus containing 2.5×10^{11} AAV8 vector genomes. The sh*Vdac1* sequences are listed in Supporting Information Table S3.

2.11. Transmission electron microscopy

Primary hepatocytes were fixed in 2.5% glutaraldehyde overnight at room temperature. Then, cells were post-fixed in potassium ferrocyanide–osmium tetroxide for 1 h and dehydrated in a bath with increasing concentrations of ethanol. After embedding and slicing, cells were staining with uranyl acetate and lead citrate. Sections were observed under a H-7650 transmission electron microscope (Hitachi Limited, Tokyo, Japan).

2.12. Detection of liver reactive oxygen species (ROS) content and ATP content

The content of ROS in liver tissue was measured using the tissue ROS test kit (HR8821; BioRab, Beijing, China) according to manufacturer's instructions and normalized to protein concentration. Briefly, fresh liver tissue was homogenized in cold buffer and centrifuged ($100 \times g$) for 5 min at 4 °C. The supernatant was used to analyze ROS content. Add 200 µL of supernatant and 2 µL of dihydroethidium probe to a 96-well plate, and mix them well. Plate was incubated at 37 °C for 30 min in dark, and then read on a Molecular Devices SpectraMax Gemini EM (Molecular Devices, Sunnyvale, CA, USA) at $\lambda_{exc} = 510$ nm and $\lambda_{emi} = 610$ nm.

The content of ATP in liver tissue was measured using the ATP colorimetric/fluorometric assay kit (K354-100; BioVision, Milpitas, CA, USA) according to manufacturer's instructions and normalized to protein concentration.

2.13. Seahorse assay

Oxygen consumption rate (OCR) was measured using the Seahorse XFe 24 Analyzer

(Agilent Technologies, Santa Clara, CA, USA). 3×10^4 hepatocytes per well were plated as a monolayer culture in Seahorse cell plates. To perform the mitochondrial stress test, 2 μmol/L oligomycin, 1.5 μmol/L FCCP, and 1 μmol/L antimycin A + 1 μmol/L rotenone were added as indicated.

2.14. Measurement of intracellular mitochondrial membrane potential and mitochondrial ROS (mtROS)

Intracellular mitochondrial membrane potential and mtROS production were visualized using the JC-1 mitochondrial membrane potential assay kit (C0008; Applygen Technologies, Beijing, China) or the MitoSOX Red Mitochondrial Superoxide Indicator (40778ES50; Yeasen Biotechnology) according to manufacturer's instruction, respectively. To measure intracellular mitochondrial membrane potential, cells were incubated with 10 μg/mL of JC-1 working solution for 20 min at 37 °C, protected from light. To measure intracellular mtROS, cells were incubated with 4.5 μmol/L of MitoSOX working solution for 10 min at 37 °C, protected from light. After incubation, cells were washed gently three times with warm buffer, and then visualized by a laser scanning confocal microscopy (Olympus FluoView 1200).

2.15. VDAC1 cross-linking assay

To detect the oligomeric forms of VDAC1, chemical cross-linking of cells was performed as described previously[39,40]. Briefly, hepatocytes were washed twice with PBS, harvested, and incubated with 0.5 mmol/L EGS (21565, ThermoScientific, Waltham, MA, USA) in PBS (pH 7.4) at 30 °C for 20 min. The pellet was lysed in NP-40 lysis buffer by sonication on ice. Samples were subjected to SDS-PAGE and immunoblotting using anti-VDAC1 antibody.

2.16. Plasmid construction

WT and truncated fragments of mouse *Nedd4-1* were amplified from mouse complementary DNA and cloned into the pcDNA3.1-HA vector. WT fragments of mouse *Vdac1* were amplified from mouse complementary DNA and cloned into the pEnCMV-3 × Flag vector. Mutant fragment of mouse NEDD4-1 (NEDD4-1^{C854S}) and PPTY deletion fragment of mouse VDAC1 (VDAC1$^{\triangle PPTY}$) were generated using Q5 Site-Directed Mutagenesis Kit (E0554S; New England BioLabs, Ipswich, MA, USA).

Each construction was verified by sequencing (Comate Bioscience, Changchun, China).

2.17. Coimmunoprecipitation (Co-IP) assay

293T cells were lysed in ice-cold NP40 lysis buffer supplemented with a protease inhibitor cocktail, and centrifuged (12,000 × g) at 4 °C for 10 min. The cell lysates were used for immunoprecipitation with Pierce Crosslink Immunoprecipitation Kit (26147, Thermo Scientific), anti-Flag M2 affinity gel (A2220, Sigma–Aldrich), or anti-HA affinity gel (E6779, Sigma–Aldrich). The obtained beads were washed five times with lysis buffer, and the immunoprecipitates were obtained by boiling in 2× loading buffer at 95 °C for 5 min, or eluted by 100 μg/mL HA peptide (I2149; Sigma–Aldrich). Finally, the immunoprecipitates and whole cell lysates were subjected to immunoblotting using the indicated primary antibodies and corresponding secondary antibodies. The details of antibodies are listed in Table S1.

2.18. Measurement of cell viability

Cell viability was detected using cell counting kit-8 (C0038; Beyotime Institute of Biotechnology) according to manufacturer's instructions.

2.19. Statistical analysis

Data were generated from multiple repeats of different biological experiments and were analyzed using the appropriate statistical analysis methods. Statistical significance of Kaplan–Meier survival curves was analyzed by log-rank test. The correlation between two parameters was analyzed by the Pearson correlation analysis. Statistical significance of the rest of data was calculated using the two-tailed unpaired Student t test, or ANOVA with Bonferroni correction. Results are presented as the mean ± standard error of mean (SEM). P value < 0.05 is considered statistically significant. Statistics were performed using GraphPad Prism software (Version 6; GraphPad Software Inc., La Jolla, CA, USA) and Statistical Package for the Social Sciences (SPSS) software (Version 19.0; SPSS Incorporated, Chicago, IL, USA).

3. Results

3.1. Hepatocyte NEDD4-1 expression is dramatically downregulated in AILI and negatively correlates with liver injury severity

10

To explore the potential role of NEDD4-1 in AILI, 6- to 8-week-old male C57BL/6N mice were administered either a nonlethal (300 mg/kg) or lethal (600 mg/kg) dose of APAP over different durations by intraperitoneal injection. Administration of APAP resulted in hepatic injury, as indicated by highly increased serum ALT and AST activities (Supporting Information Fig. S1A and S1B). Typical features of liver injury and centrilobular hepatocellular necrosis were also observed by H&E staining in APAP-treated mice (Fig. S1C).

The protein (Fig. 1A and B) and mRNA (Fig. 1C) abundances of NEDD4-1 were markedly reduced in time- and dose-dependent manners in the livers of APAP-challenged mice. In addition, hepatic *Nedd4-1* mRNA expression was negatively correlated with serum ALT and AST activities, as determined by Pearson correlation analysis (Fig. 1D and E). Due to the cellular heterogeneity of liver tissue, we analyzed a publicly available single-cell RNA-seq dataset derived from normal human livers (GSE192742; https://www.livercellatlas.org/index.php)[41] and found that *NEDD4-1* was predominantly expressed in hepatocytes and, to a lesser extent, in cholangiocytes, endothelial cells, and stromal cells (Fig. S1D). These four types of cells were thus isolated from the livers of mice administered saline or APAP. The NEDD4-1 protein abundance was lower in hepatocytes but not in other cell types from APAP-treated mice (Fig. S1E), suggesting that APAP overdose selectively decreases the abundance of NEDD4-1 in hepatocytes. Similarly, *in vitro*, APAP treatment downregulated NEDD4-1 expression in WT hepatocytes in time- and dose-dependent manners (Fig. 1F and G; Fig. S1F). The decrease of NEDD4-1 abundance in APAP-treated mouse primary hepatocytes was also confirmed by immunofluorescence analyses (Fig. 1H). These results suggest a potential regulatory role of NEDD4-1 in APAP-induced hepatotoxicity.

Insert Fig. 1

3.2. Hepatocyte NEDD4-1 deficiency exacerbates APAP-induced liver injury and necrosis

To understand the role of NEDD4-1 in the liver and the mechanism by which its downregulation contributes to AILI pathogenesis, we generated mice with hepatocyte-specific *Nedd4-1* knockout (hereafter referred to as HepKO mice) (Supporting Information Fig. S2A). Western blot analysis confirmed the specific knockout of NEDD4-1 in the livers of HepKO mice (Fig. S2B). Unchallenged HepKO mice were

healthy and fertile without noticeable gross phenotypes and demonstrated no significant differences in body weight (Fig. S2C) and the liver weight/body weight ratio (Fig. S2D) compared with those of their Flox counterparts. However, under challenge with 300 mg/kg APAP, NEDD4-1 loss led to more severe liver injury, as indicated by the higher serum ALT (Fig. 2A), AST (Fig. 2B), and LDH (Fig. 2C) activities. In addition, hepatocyte NEDD4-1 deficiency evidently exacerbated the APAP-induced increase in the serum level of HMGB1 (Fig. 2D), a nuclear protein released extracellularly from necrotic cells[42-44]. H&E staining (Fig. 2E) and evaluation of gross liver appearance (Fig. S2E) further confirmed the enhancement of APAP-induced liver injury and necrosis in APAP-treated HepKO mice. In particular, HepKO mice had a much lower survival rate than Flox mice after treatment with a lethal dose (600 mg/kg) of APAP (Fig. 2F). In addition, identical protein abundances of CYP2E1 (Fig. S2F) and GSH levels (Fig. S2G) were observed in the livers of APAP-treated Flox and HepKO mice, indicating unaffected APAP metabolism. Taken together, these results indicate that hepatocyte-specific NEDD4-1 deficiency exacerbates APAP-induced liver injury and necrosis.

To gain better insight into the pathological alterations initiated by hepatocyte NEDD4-1 deficiency in the AILI setting, we performed RNA-seq using liver samples from APAP-treated Flox and HepKO mice. Unsupervised hierarchical clustering showed that liver samples from these two groups were clearly separated (Supporting Information Fig. S3A), with 1201 upregulated and 736 downregulated genes (Fig. 2G, Supporting Information Table S4) in the APAP-treated HepKO group. GSEA revealed that the upregulated genes were associated with the chemokine, inflammasome, DNA damage, tumor necrosis factor signaling, and cell death pathways (Fig. 2H, red; Fig. S3B). In addition, mitochondrial function-related genes associated with fatty acid oxidation and mitochondrial translation were downregulated (Fig. 2H, gray; Fig. S3B). These RNA-seq data further demonstrate the negative effects of NEDD4-1 deficiency on AILI.

For further *in vitro* experiments, hepatocytes were isolated from HepKO and Flox mice (Supporting Information Fig. S4) and were then exposed to APAP. NEDD4-1 deletion in hepatocytes markedly exacerbated APAP-induced hepatocyte death, as determined by Calcein-AM/PI double staining (Fig. 2I), an LDH release assay (Fig. 2J) and measurement of the HMGB1 concentration in the culture medium (Fig. 2K). Taken together, these *in vivo* and *in vitro* results reveal that loss of hepatocyte NEDD4-1

exacerbates APAP-induced liver injury and necrosis.

Insert Fig. 2

3.3. Overexpression of hepatocyte NEDD4-1 alleviates APAP-induced liver injury and necrosis

To further confirm the function of hepatocyte NEDD4-1 in AILI, we generated mice with hepatocyte NEDD4-1 overexpression using AAV8 delivering hepatocyte-specific promoter TBG and full-length *Nedd4-1* gene sequence (AAV8-NEDD4-1), and examined their response to APAP treatment (Supporting Information Fig. S5A). Western blot analysis confirmed the overexpression of NEDD4-1 in the livers of AAV8-NEDD4-1-injected mice (Fig. S5B). The similar levels of CYP2E1 protein abundance (Fig. S5C) and GSH depletion (Fig. S5D) indicated that APAP metabolism was not influenced by AAV8-NEDD4-1 injection. Compared to AAV8-Control-injected mice, AAV8-NEDD4-1-injected mice showed alleviation of liver injury and necrosis in response to APAP challenge, as indicated by the decreased necrotic area (Fig. 3A); decreased serum ALT (Fig. 3B), AST (Fig. 3C) and LDH (Fig. 3D) activities; and reduced serum HMGB1 level (Fig. 3E). Moreover, AAV8-mediated hepatocyte NEDD4-1 overexpression was sufficient to increase the mouse survival rate upon administration of a lethal dose (600 mg/kg) of APAP (Fig. 3F).

For *in vitro* experiments, primary hepatocytes obtained from WT mice were transfected with adenovirus containing the NEDD4-1 plasmid or control vector (Fig. S5E) and then exposed to APAP. Consistent with the *in vivo* results, APAP-induced cell death was also alleviated by NEDD4-1 overexpression in primary hepatocytes, as indicated by the decreased cell death rate (PI positive cells %; Fig. 3G), level of LDH release (Fig. 3H), and concentration of HMGB1 in the culture medium (Fig. 3I). Based on the combined *in vivo* and *in vitro* results, we conclude that hepatocyte NEDD4-1 overexpression ameliorates APAP-induced liver injury and necrosis.

Insert Fig. 3

3.4. NEDD4-1 mediates APAP-induced hepatocyte mitochondrial damage

Our RNA-seq data demonstrate an enhanced defect in mitochondrial function in APAP-treated HepKO mice. Therefore, we investigated the influence of NEDD4-1 on mitochondrial homeostasis in the setting of AILI by determining the ATP and ROS contents, mitochondrial membrane potential, mitochondrial membrane

permeabilization, etc. APAP-induced hepatic ATP depletion (Fig. 4A), ROS overproduction (Fig. 4B), and cytosolic leakage of mitochondrial intermembrane proteins (apoptosis-inducing factor [AIF], endonuclease G [Endo G] and cytochrome *c* [Cyt C]; Fig. 4C) were aggravated by hepatocyte NEDD4-1 knockout *in vivo*, indicating that hepatocyte NEDD4-1 deficiency exacerbated APAP-induced mitochondrial damage. Conversely, overexpression of hepatocyte NEDD4-1 by AAV8-NEDD4-1 injection caused a beneficial improvement in APAP-induced mitochondrial damage (Supporting Information Fig. S6A–S6C).

In vitro, transmission electron microscopy revealed mitochondrial swelling and damage in APAP-treated Flox hepatocytes, which was even worse in APAP-treated HepKO hepatocytes (Fig. 4D). In addition, upon APAP treatment, HepKO hepatocytes displayed greater increases in the cytosolic release of mitochondrial intermembrane proteins (AIF, Endo G and Cyt C) than Flox hepatocytes (Fig. 4E). OCR measurements obtained by a Seahorse assay demonstrated that the impairment of basal respiration, ATP production and maximal respiration induced by APAP exposure were further aggravated by hepatocyte NEDD4-1 ablation, revealing a more severe defect in mitochondrial function (Fig. 4F). JC-1 staining, which is used to visualize the mitochondrial membrane potential by detecting fluorescence, indicated that NEDD4-1 ablation in primary hepatocytes aggravated the APAP-induced collapse of the mitochondrial membrane potential (Fig. 4G). Meanwhile, MitoSOX staining was performed to evaluate mtROS production *in vitro* and showed that knockout of NEDD4-1 in hepatocytes increased APAP-induced overproduction of mtROS (Fig. 4H). In contrast, transfection of NEDD4-1 adenovirus into WT primary hepatocytes significantly mitigated APAP-induced mitochondrial damage, as evidenced by the Seahorse assay (Fig. S6D), JC-1 staining (Fig. S6E), and MitoSOX staining (Fig. S6F).

In summary, these gain- and loss-of-function studies *in vivo* and *in vitro* show that hepatocyte NEDD4-1 at least partially mediates APAP-induced hepatocyte mitochondrial damage.

Insert Fig. 4

3.5. Knockdown of VDAC1 mitigates the enhanced AILI events caused by hepatocyte NEDD4-1 deficiency

The striking effect of NEDD4-1 on mitochondrial intermembrane protein leakage in the

setting of AILI prompted us to investigate the influence of NEDD4-1 on proteins related to mitochondrial membrane permeabilization. Intriguingly, under APAP treatment, hepatocyte NEDD4-1 ablation increased the mitochondrial translocation of phosphorylated JNK (P-JNK) and the protein abundance of mitochondrial VDAC1, but had a negligible influence on the protein abundance of mitochondrial bcl-2-associated X (Bax) and cyclophilin D (CYPD) (Fig. 5A). In contrast, NEDD4-1 overexpression resulted in the opposite trends in the protein levels of mitochondrial P-JNK and VDAC1 in APAP-treated primary hepatocytes (Supporting Information Fig. S7A).

Since NEDD4-1 markedly influenced the VDAC1 protein abundance in the setting of AILI, we sought to determine whether VDAC1 participates in the regulation of NEDD4-1 in AILI pathogenesis. First, the expression profile of hepatic VDAC1 in the setting of AILI was determined. Results showed that the VDAC1 protein abundance was markedly increased in the livers of APAP-challenged mice (Fig. 5B and C) and in APAP-treated primary hepatocytes (Fig. S7B), although VDAC1 mRNA expression did not differ significantly (Fig. 5D), suggesting that the increase in the VDAC1 protein abundance upon APAP treatment was not due to changes in transcription.

To further elucidate the role of VDAC1 in NEDD4-1-regulated AILI, VDAC1 was silenced in Flox and HepKO mice *via* tail vein injection of AAV8-shVDAC1, and the mice were then exposed to APAP (Supporting Information Fig. S8A). The silencing efficiency of AAV8-shVDAC1 in HepKO mice was validated by Western blotting (Fig. S8B). AAV8-shVDAC1 injection did not affect the CYP2E1 protein abundance (Fig. S8C) and GSH depletion (Fig. S8D), indicating unaffected APAP metabolism. Nevertheless, AAV8-shVDAC1 injection significantly alleviated liver injury and necrosis both in APAP-treated Flox mice and in APAP-treated HepKO mice compared with their corresponding controls, as indicated by H&E staining (Fig. 5E); serum ALT (Fig. 5F), AST (Fig. 5G), LDH activities (Fig. 5H); HMGB1 levels (Fig. 5I); and gross liver appearance (Fig. S8E). Consistent with these findings, the reduction in the survival rate was ameliorated by VDAC1 knockdown (Fig. 5J). Moreover, hepatic mitochondrial damage was alleviated by injection of AAV8-shVDAC1 (Fig. 5K and L). Notably, the mitochondrial translocation of P-JNK induced by NEDD4-1 deficiency under APAP exposure was reduced by VDAC1 knockdown, suggesting that VDAC1 may function cooperatively with JNK (Fig. 5M). Collectively, these results show that knockdown of VDAC1 effectively alleviates APAP-induced mitochondrial damage,

liver injury and necrosis. More importantly, the enhanced AILI events caused by hepatocyte NEDD4-1 deficiency were also weakened by VDAC1 knockdown *in vivo*. These *in vivo* phenomena were also evaluated *in vitro* in HepKO hepatocytes treated with APAP and Ad-shVDAC1 (Fig. S8F). Under APAP exposure, the cell death rate (PI positive cells %; Fig. 6A), LDH release (Fig. 6B) and HMGB1 concentration in the culture medium (Fig. 6C) were lower in the Ad-shVDAC1 group than in the Ad-shControl group. Furthermore, mitochondrial damage enhanced by hepatocyte NEDD4-1 knockout was also mitigated by VDAC1 knockdown under APAP treatment *in vitro*, as determined by a Seahorse assay (Fig. 6D), JC-1 staining (Fig. 6E), and MitoSOX staining (Fig. 6F). These data indicate that knockdown of VDAC1 protects against the enhancement of APAP-induced pathological events resulting from hepatocyte NEDD4-1 deficiency *in vitro*.

Insert Figs. 5 and 6

As a recent study revealed that VDAC1 oligomerization mediates APAP toxicity[45], we further investigated whether NEDD4-1 affects VDAC1 oligomerization in APAP toxicity. *In vitro* experiments showed that NEDD4-1 knockout promoted APAP-induced VDAC1 oligomerization (Supporting Information Fig. S9A), which was reduced by NEDD4-1 overexpression (Fig. S9B). These results indicate that NEDD4-1 regulates VDAC1 oligomerization in APAP toxicity.

3.6. Identification of VDAC1 as a functional ubiquitination substrate of NEDD4-1

Since the increase in the VDAC1 protein abundance upon APAP treatment was not due to transcriptional changes, we rationally deduced that in the setting of AILI, VDAC1 is regulated through proteasomal degradation *via* the E3 ubiquitin ligase NEDD4-1. As expected, NEDD4-1 overexpression significantly decreased the protein abundance of VDAC1, and this effect was blocked by the proteasome inhibitor MG132 but not by the lysosome inhibitor CQ, emphasizing that NEDD4-1 regulates the proteasomal degradation of VDAC1 (Fig. 7A).

The interaction of exogenous NEDD4-1 with VDAC1 was demonstrated by reciprocal Co-IP (Fig. 7B, C). Consistently, intracellular colocalization of endogenous NEDD4-1 and VDAC1 was further observed in primary hepatocytes *via* an immunofluorescence colocalization assay (Fig. 7D). Subsequently, molecular mapping assays using WT and truncated fragments of NEDD4-1 revealed that the WW domain

of NEDD4-1 is responsible for its interaction with VDAC1 (Fig. 7E). Moreover, missing PPTY motif in VDAC1 abolished its interaction with NEDD4-1 (Fig. 7F). Taken together, these results clarify that NEDD4-1 binds to the PPTY motif of VDAC1 through its WW domain.

Next, we investigated whether NEDD4-1 promotes the ubiquitination of VDAC1. As shown in the ubiquitination assays, NEDD4-1 significantly facilitated the ubiquitination of VDAC1 (Fig. 7G and H), but the NEDD4-1^{C854S} mutant lacking ubiquitin ligase activity did not (Fig. 7H). These results indicate that NEDD4-1-catalyzed ubiquitination of VDAC1 depends on its E3 ubiquitin ligase activity. Screening for potential lysine ubiquitination types revealed that both WT and K48O (ubiquitin with the intact Lys48 residue only) ubiquitin but not K6O, K11O, K27O, K33O, or K63O (Fig. 7I) could be linked to VDAC1 by NEDD4-1. Moreover, NEDD4-1 failed to link K48R ubiquitin (ubiquitin with mutation of Lys48) to VDAC1 (Fig. 7J). Investigation using a K48 linkage-specific anti-ubiquitin antibody further confirmed that NEDD4-1 facilitated K48-linked ubiquitination of VDAC1 (Fig. 7K). In summary, the present data indicate that NEDD4-1 directly interacts with VDAC1 and predominantly promotes K48-linked ubiquitination of VDAC1, eventually resulting in its degradation.

Insert Fig. 7

Accordingly, we propose a signaling mechanism in which VDAC1 is targeted as a degradation substrate of NEDD4-1 to mediate hepatocyte mitochondrial damage and necrosis during AILI (Fig. 8).

Insert Fig. 8

4. Discussion

Hepatotoxicity limits the clinical utility of APAP, although it remains the most ubiquitous over-the-counter antipyretic and analgesic worldwide[5]. APAP hepatotoxicity accounts for several fold more deaths related to acute liver failure than hepatotoxicity from all other prescription drugs combined[3]. However, there is currently no standard antidote to treat AILI except for *N*-acetylcysteine, which has certain limitations. Therefore, exploring the mechanisms by which APAP causes toxicity is essential to combat AILI with appropriate therapies. Here, we identified NEDD4-1 as a new and robust suppressor of AILI that functions to maintain hepatocyte mitochondrial homeostasis and protect against hepatic necrosis. Furthermore, VDAC1 was identified

as a degradation substrate protein that mediates the downstream protective effects of NEDD4-1 against AILI. Considering these results, targeting the NEDD4-1–VDAC1 axis could be a feasible therapeutic strategy for AILI.

The E3 ubiquitin ligase NEDD4-1 has attracted extensive attention in recent decades for its vital role in regulating a diverse range of physiological processes and human diseases[19-22]. Accumulating evidence has validated the protective effect of NEDD4-1 against tissue injury, such as hepatic and cardiac ischemia/reperfusion injury[21,25,26]. However, the role of NEDD4-1 in regulating drug-induced liver injury has not been described previously. Here, we found that hepatic NEDD4-1 expression was dramatically downregulated in AILI. Notably, HepKO mice showed higher mortality and more severe liver injury upon APAP overdose, while mice overexpressing NEDD4-1 exhibited alleviation of the response to APAP exposure, identifying NEDD4-1 as exerting protective effects against AILI. In addition, this conclusion was also supported by our *in vitro* findings.

AILI has a complex pathogenesis that involves multiple pathogenic events. The initiating event begins with the generation of NAPQI[7,8,46], which then binds covalently to proteins, especially mitochondrial proteins. Widespread covalent binding results in cellular oxidative stress, mitochondrial dysfunction, DNA fragmentation, etc., culminating in necrosis and liver injury[11,47,48]. In this study, the RNA-seq data suggest that NEDD4-1 deficiency is implicated in multiple pathogenic pathways (oxidative stress, mitochondrial dysfunction, DNA damage and cell death) during AILI progression, all of which are closely related to mitochondria—the primary intracellular organelle targeted by APAP[49]. In particular, our loss- and gain-of-function experiments further demonstrated that NEDD4-1 at least partially mediates APAP-induced hepatocyte mitochondrial damage and necrosis. Therefore, mitochondrial damage is a critical pathological event in NEDD4-1 deficiency-mediated exacerbation of APAP hepatotoxicity.

The mitochondrial outer membrane is a functional barrier that physically separates mitochondria from the cytosol and orchestrates mitochondrial homeostasis[50]. VDAC1 is the most abundant gatekeeper in the mitochondrial outer membrane and forms pores that control the exchange of metabolites, nucleotides, ions, and small molecules between mitochondria and the cytosol[51-53]. Genetic alteration, abnormal expression, translocation, oligomerization and ubiquitination of VDAC1 regulate various cellular

18

pathological processes, such as mitochondrial outer membrane permeabilization, mitochondrial DNA release, mitochondrial intermembrane protein release, mtROS production, and cell death[52,54-56]. All of these pathological processes have been validated to be major players in the pathogenesis of AILI, foreshadowing VDAC1 may participate in AILI progression. Indeed, our results provided evidence for the elevation of VDAC1 abundance as a result of AILI, which was supported by mitochondrial proteomic data[57]. It is noteworthy that VDAC is sometimes used as a mitochondrial reference protein. Nevertheless, our findings and those of other functional studies[58-62] of VDAC1 suggested that the usage of VDAC as a mitochondrial reference protein should be exercised cautiously or validated in different contexts. Here, our subsequent experiments show that VDAC1 participates in AILI progression and that its abnormal accumulation is at least partially responsible for NEDD4-1 deficiency-mediated exacerbation of AILI. Specifically, in our study, VDAC1 knockdown significantly alleviated mitochondrial damage, necrosis and liver injury, which is most likely achieved through decreasing VDAC1 oligomerization as a recent study ascertained[45]. Mechanistically, we demonstrate that NEDD4-1 binds to the PPTY motif of VDAC1 through its WW domain, subsequently catalyzing K48-linked ubiquitination of VDAC1 and ultimately resulting in VDAC1 degradation. A recent study concerning drug resistance in melanoma cells during cancer therapy further supported the idea that VDAC1 is a degradation substrate of NEDD4-1[58]. Taken together, our data indicate that targeting VDAC1 for degradation is the primary cellular mechanism by which NEDD4-1 performs a beneficial function in AILI.

Among the complex molecular networks coordinating APAP hepatotoxicity, JNK is a star molecule due to its comprehensive regulation of mitochondrial homeostasis. Activation and mitochondrial translocation are the prerequisites for JNK to exert its detrimental effects on AILI progression (Supporting Information Fig. S10)[63-66]. Our study showed that ablation of hepatocyte NEDD4-1 enhanced the APAP-induced mitochondrial translocation of activated JNK, which was reduced by silencing of VDAC1. Convincing evidence indicates that VDAC1 mediates the cytosolic transport of superoxide anion and peroxynitrite[67], whose presence in the cytosol enables the activation of JNK, ultimately amplifying mitochondrial dysfunction[68]. Thus, JNK may act as one of the executors responding to NEDD4-1–VDAC1 axis in the setting of AILI. However, further research on the exact regulatory mechanism linking the NEDD4-1–

VDAC1 axis and JNK translocation is required.

5. Conclusions

Overall, the present study identifies that by facilitating ubiquitination-mediated degradation of VDAC1 in hepatocytes, NEDD4-1 attenuates AILI (Fig. 8). This fact makes NEDD4-1–VDAC1 axis a promising target for AILI therapy. Our collective findings provide further insights into AILI progression and offer new possibilities for therapies targeting this disease and its related pathologies.

Acknowledgments

Author contributions

Yiwei Zhu: conceptualization, validation, formal analysis, investigation, visualization, and writing-original draft; Lin Lei: conceptualization, formal analysis, investigation, and writing-review and editing; Xinghui Wang, Linfang Chen: validation, investigation, and writing-review and editing; Wei Li, Jinxia Li, Chenchen Zhao: investigation, and writing-review and editing; Xiliang Du, Yuxiang Song, Wenwen Gao: writing-review and editing; Guowen Liu: conceptualization, resources, writing-review and editing, and funding acquisition; Xinwei Li: conceptualization, resources, writing-review and editing, supervision, project administration, and funding acquisition.

Conflicts of interest

The authors declare no conflicts of interest.

References

1. Bernal W, Williams R. Acute liver failure. *Clin Liver Dis* 2020;**16**:45-55.
2. Jaeschke H, Adelusi OB, Akakpo JY, Nguyen NT, Sanchez-Guerrero G, Umbaugh DS, et al. Recommendations for the use of the acetaminophen hepatotoxicity model for mechanistic studies and how to avoid common pitfalls. *Acta Pharm Sin B* 2021; **11**: 3740-55.
3. Lee WM. Acetaminophen (APAP) hepatotoxicity—isn't it time for APAP to go

away?. *J Hepatol* 2017; **67**: 1324-31.

4. Bernal W, Auzinger G, Dhawan A, Wendon J. Acute liver failure. *Lancet* 2010; **376**: 190-201.

5. Stravitz RT, Lee WM. Acute liver failure. *Lancet* 2019; **394**: 869-81.

6. McGill MR, Jaeschke H. Metabolism and disposition of acetaminophen: recent advances in relation to hepatotoxicity and diagnosis. *Pharm Res* 2013; **30**: 2174-87.

7. Dahlin DC, Miwa GT, Lu AY, Nelson SD. *N*-Acetyl-*p*-benzoquinone imine: a cytochrome P-450-mediated oxidation product of acetaminophen. *Proc Natl Acad Sci U S A* 1984; **81**: 1327-31.

8. McGill MR, Williams CD, Xie Y, Ramachandran A, Jaeschke H. Acetaminophen-induced liver injury in rats and mice: comparison of protein adducts, mitochondrial dysfunction, and oxidative stress in the mechanism of toxicity. *Toxicol Appl Pharmacol* 2012; **264**: 387-94.

9. Lancaster EM, Hiatt JR, Zarrinpar A. Acetaminophen hepatotoxicity: an updated review. *Arch Toxicol* 2015; **89**: 193-9.

10. Jaeschke H, McGill MR, Ramachandran A. Oxidant stress, mitochondria, and cell death mechanisms in drug-induced liver injury: lessons learned from acetaminophen hepatotoxicity. *Drug Metab Rev* 2012; **44**: 88-106.

11. Yan M, Huo Y, Yin S, Hu H. Mechanisms of acetaminophen-induced liver injury and its implications for therapeutic interventions. *Redox Biol* 2018; **17**: 274-83.

12. Hershko A, Ciechanover A. The ubiquitin system. *Annu Rev Biochem* 1998; **67**: 425-79.

13. Haglund K, Dikic I. Ubiquitylation and cell signaling. *EMBO J* 2005; **24**: 3353-9.

14. Swatek KN, Komander D. Ubiquitin modifications. *Cell Res* 2016; **26**: 399-422.

15. Berndsen CE, Wolberger C. New insights into ubiquitin E3 ligase mechanism. *Nat Struct Mol Biol* 2014; **21**: 301-7.

16. Zheng N, Shabek N. Ubiquitin ligases: structure, function, and regulation. *Annu Rev Biochem* 2017; **86**: 129-57.

17. Chen D, Gehringer M, Lorenz S. Developing small-molecule inhibitors of HECT-type ubiquitin ligases for therapeutic applications: challenges and opportunities. *Chembiochem* 2018; **19**: 2123-35.

18. Rotin D, Kumar S. Physiological functions of the HECT family of ubiquitin ligases. *Nat Rev Mol Cell Biol* 2009; **10**: 398-409.

19. Huang X, Chen J, Cao W, Yang L, Chen Q, He J, et al. The many substrates and functions of NEDD4-1. *Cell Death Dis* 2019; **10**: 904.

20. He H, Huang C, Chen Z, Huang H, Wang X, Chen J. An outlined review for the role of Nedd4-1 and Nedd4-2 in lung disorders. *Biomed Pharmacother* 2020; **125**: 109983.

21. Zhang Y, Qian H, Wu B, You S, Wu S, Lu S, et al. E3 ubiquitin ligase NEDD4 family regulatory network in cardiovascular disease. *Int J Biol Sci* 2020; **16**: 2727-40.

22. Zou X, Levy-Cohen G, Blank M. Molecular functions of NEDD4 E3 ubiquitin ligases in cancer. *Biochim Biophys Acta* 2015; **1856**: 91-106.

23. Liu Q, Zhang S, Sun Z, Guo X, Zhou H. E3 ubiquitin ligase Nedd4 is a key negative regulator for non-canonical inflammasome activation. *Cell Death Differ* 2019; **26**: 2386-99.

24. Bachofner M, Speicher T, Bogorad RL, Muzumdar S, Derrer CP, Hurlimann F, et al. Large-scale quantitative proteomics identifies the ubiquitin ligase Nedd4-1 as an essential regulator of liver regeneration. *Dev Cell* 2017; **42**: 616-25.

25. Zhou J, Hu M, He M, Wang X, Sun D, Huang Y, et al. TNFAIP3 interacting protein 3 is an activator of Hippo-YAP signaling protecting against hepatic ischemia/reperfusion injury. *Hepatology* 2021; **74**: 2133-53.

26. Hu W, Zhang P, Gu J, Yu Q, Zhang D. NEDD4-1 protects against ischaemia/reperfusion-induced cardiomyocyte apoptosis *via* the PI3K/Akt pathway. *Apoptosis* 2017; **22**: 437-48.

27. Wang ZW, Hu X, Ye M, Lin M, Chu M, Shen X. NEDD4 E3 ligase: functions and mechanism in human cancer. *Semin Cancer Biol* 2020; **67**: 92-101.

28. Malato Y, Naqvi S, Schuermann N, Ng R, Wang B, Zape J, et al. Fate tracing of mature hepatocytes in mouse liver homeostasis and regeneration. *J Clin Invest* 2011; **121**: 4850-60.

29. Chao X, Wang S, Fulte S, Ma X, Ahamed F, Cui W, et al. Hepatocytic p62 suppresses ductular reaction and tumorigenesis in mouse livers with mTORC1 activation and defective autophagy. *J Hepatol* 2022; **76**: 639-51.

30. Isabel Hernandez-Alvarez M, Sebastian D, Vives S, Ivanova S, Bartoccioni P, Kakimoto P, et al. Deficient endoplasmic reticulum-mitochondrial phosphatidylserine transfer causes liver disease. *Cell* 2019; **177** :881-95.

31. Wang L, Yu J, Zhou Q, Wang X, Mukhanova M, Du W, et al. TOX4, an insulin receptor-independent regulator of hepatic glucose production, is activated in diabetic liver. *Cell Metab* 2022; **34**: 158-70.

32. Zhu YW, Liu GW, Du XL, Shi Z, Jin MY, Sha XY, et al. Expression patterns of hepatic genes involved in lipid metabolism in cows with subclinical or clinical ketosis. *J Dairy Sci* 2019; **102**: 1725-35.

33. Bustin SA, Benes V, Garson JA, Hellemans J, Huggett J, Kubista M, et al. The MIQE guidelines: minimum information for publication of quantitative real-time PCR experiments. *Clin Chem* 2009; **55**: 611-22.

34. Livak KJ, Schmittgen TD. Analysis of relative gene expression data using real-time quantitative PCR and the $2^{-\Delta\Delta CT}$ method. *Methods* 2001; **25**: 402-8.

35. Charni-Natan M, Goldstein I. Protocol for primary mouse hepatocyte isolation. *STAR Protoc* 2020; **1**: 100086.

36. Gonzalez-Sanchez E, Firrincieli D, Housset C, Chignard N. Expression patterns of nuclear receptors in parenchymal and non parenchymal mouse liver cells and their modulation in cholestasis. *Biochimica Et Biochim Biophys Acta Mol Basis Dis* 2017; **1863**: 1699-708.

37. Loeuillard E, El Mourabit H, Lei L, Lemoinne S, Housset C, Cadoret A. Endoplasmic reticulum stress induces inverse regulations of major functions in portal myofibroblasts during liver fibrosis progression. *Biochim Biophys Acta Mol Basis Dis* 2018; **1864**: 3688-96.

38. Schindelin J, Arganda-Carreras I, Frise E, Kaynig V, Longair M, Pietzsch T, et al. Fiji: an open-source platform for biological-image analysis. *Nat Methods* 2012; **9**: 676-82.

39. Nagakannan P, Islam MI, Karimi-Abdolrezaee S, Eftekharpour E. Inhibition of VDAC1 protects against glutamate-induced oxytosis and mitochondrial fragmentation in hippocampal HT22 cells. *Cell Mol Neurobiol* 2019; **39**: 73-85.

40. Keinan N, Tyomkin D, Shoshan-Barmatz V. Oligomerization of the mitochondrial protein voltage-dependent anion channel is coupled to the induction of apoptosis. *Mol Cell Biol* 2010; **30**: 5698-709.

41. Guilliams M, Bonnardel J, Haest B, Vanderborght B, Wagner C, Remmerie A, et al. Spatial proteogenomics reveals distinct and evolutionarily conserved hepatic macrophage niches. *Cell* 2022; **185**: 379-96.

42. Scaffidi P, Misteli T, Bianchi ME. Release of chromatin protein HMGB1 by necrotic cells triggers inflammation. *Nature* 2010; **467**: 622.

43. Takano K, Shinoda M, Tanabe M, Miyasho T, Yamada S, Ono S, et al. Protective effect of high-mobility group box 1 blockade on acute liver failure in rats. *Shock* 2010; **34**: 573-9.

44. Chen DS, Ni HM, Wang L, Ma XW, Yu J, Ding WX, et al. p53 up-regulated modulator of apoptosis induction mediates acetaminophen-induced necrosis and liver injury in mice. *Hepatology* 2019; **69**: 2164-79.

45. Niu B, Lei X, Xu Q, Ju Y, Xu D, Mao L, et al. Protecting mitochondria *via* inhibiting VDAC1 oligomerization alleviates ferroptosis in acetaminophen-induced acute liver injury. *Cell Biol Toxicol* 2021; **38**: 505-30.

46. Qian H, Bai Q, Yang X, Akakpo JY, Ji L, Yang L, et al. Dual roles of p62/SQSTM1 in the injury and recovery phases of acetaminophen-induced liver injury in mice. *Acta Pharm Sin B* 2021; **11**: 3791-805.

47. Ramachandran A, Jaeschke H. Acetaminophen hepatotoxicity. *Semin Liver Dis* 2019; **39**: 221-34.

48. Chan JCY, Soh ACK, Kioh DYQ, Li J, Verma C, Koh SK, et al. Reactive metabolite-induced protein glutathionylation: a potentially novel mechanism underlying acetaminophen hepatotoxicity. *Mol Cell Proteomics* 2018; **17**: 2034-50.

49. Ramachandran A, Jaeschke H. A mitochondrial journey through acetaminophen hepatotoxicity. *Food Chem Toxicol* 2020; **140**: 111282.

50. Colombini M. Ceramide channels and mitochondrial outer membrane permeability. *J Bioenerg Biomembr* 2017; **49**: 57-64.

51. Lee AC, Xu X, Blachly-Dyson E, Forte M, Colombini M. The role of yeast VDAC genes on the permeability of the mitochondrial outer membrane. *J Membrane Biol* 1998; **161**: 173-81.

52. Xu X, Decker W, Sampson MJ, Craigen WJ, Colombini M. Mouse VDAC isoforms expressed in yeast: channel properties and their roles in mitochondrial outer membrane permeability. *J Membrane Biol* 1999; **170**: 89-102.

53. Camara AKS, Zhou Y, Wen PC, Tajkhorshid E, Kwok WM. Mitochondrial VDAC1: a key gatekeeper as potential therapeutic target. *Front Physiol* 2017; **8**: 460.

54. Zhou R, Yazdi AS, Menu P, Tschopp J. A role for mitochondria in NLRP3 inflammasome activation. *Nature* 2011; **469**: 221-5.

55. Kim J, Gupta R, Blanco LP, Yang ST, Shteinfer-Kuzmine A, Wang KN, et al. VDAC oligomers form mitochondrial pores to release mtDNA fragments and promote lupus-like disease. *Science* 2019; **366**: 1531-6.

56. Shoshan-Barmatz V, Krelin Y, Shteinfer-Kuzmine A. VDAC1 functions in Ca^{2+} homeostasis and cell life and death in health and disease. *Cell Calcium* 2018; **69**: 81-100.

57. Stamper BD, Mohar I, Kavanagh TJ, Nelson SD. Proteomic analysis of acetaminophen-induced changes in mitochondrial protein expression using spectral counting. *Chem Res Toxicol* 2011; **24**: 549-58.

58. Yang Y, Luo M, Zhang K, Zhang J, Gao T, Connell DO, et al. Nedd4 ubiquitylates VDAC2/3 to suppress erastin-induced ferroptosis in melanoma. *Nat Commun* 2020; **11**: 433.

59. Yagoda N, von Rechenberg M, Zaganjor E, Bauer AJ, Yang WS, Fridman DJ, et al. RAS–RAF–MEK-dependent oxidative cell death involving voltage-dependent anion channels. *Nature* 2007; **447**: 864-8.

60. Cuadrado-Tejedor M, Vilarino M, Cabodevilla F, Del Rio J, Frechilla D, Perez-Mediavilla A. Enhanced expression of the voltage-dependent anion channel 1 (VDAC1) in Alzheimer's disease transgenic mice: an insight into the pathogenic effects of amyloid-beta. *J Alzheimers Dis* 2011; **23**: 195-206.

61. Verma A, Pittala S, Alhozeel B, Shteinfer-Kuzmine A, Ohana E, Gupta R, et al. The role of the mitochondrial protein VDAC1 in inflammatory bowel disease: a potential therapeutic target. *Mol Ther* 2022; **30**: 726-44.

62. Mazure NM. VDAC in cancer. *Biochim Biophys Acta Bioenerg* 2017; **1858**: 665-673.

63. Gunawan BK, Liu ZX, Han D, Hanawa N, Gaarde WA, Kaplowitz N. c-Jun N-terminal kinase plays a major role in murine acetaminophen hepatotoxicity. *Gastroenterology* 2006; **131**: 165-78.

64. Hanawa N, Shinohara M, Saberi B, Gaarde WA, Han D, Kaplowitz N. Role of JNK translocation to mitochondria leading to inhibition of mitochondria bioenergetics in acetaminophen-induced liver injury. *J Biol Chem* 2008; **283**: 13565-77.

65. Henderson NC, Pollock KJ, Frew J, Mackinnon AC, Flavell RA, Davis RJ, et al. Critical role of c-Jun (NH2) terminal kinase in paracetamol-induced acute liver failure. *Gut* 2007; **56**: 982-90.

66. Latchoumycandane C, Goh CW, Ong MMK, Boelsterli UA. Mitochondrial protection by the JNK inhibitor leflunomide rescues mice from acetaminophen-induced liver injury. *Hepatology* 2007; **45**: 412-21.

67. Denicola A, Souza JM, Radi R. Diffusion of peroxynitrite across erythrocyte membranes. *Proc Natl Acad Sci U S A* 1998; **95**: 3566-71.

68. Ramachandran A, Jaeschke H. Acetaminophen hepatotoxicity: a mitochondrial perspective. *Adv Pharmacol* 2019; **85**: 195-219.

Figure captions
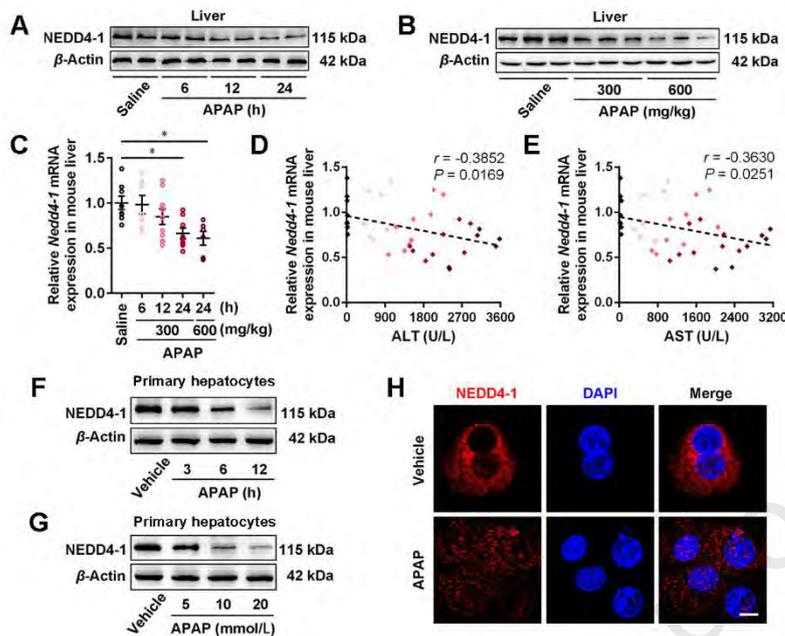
Figure 1 Hepatocyte NEDD4-1 expression is dramatically downregulated in AILI and negatively correlates with liver injury severity. (A, B) Representative Western blots of indicated proteins in livers of mice. (C) The mRNA expression of *Nedd4-1* in livers of mice. (D, E) Pearson correlation analyses showing the correlations between *Nedd4-1* mRNA level and ALT activity (D), or AST activity (E); n = 38. (F, G) Representative Western blots of indicated proteins in primary hepatocytes treated with 10 mmol/L APAP for different times (3, 6 or 12 h), or different concentrations (5, 10 or 20 mmol/L) of APAP for 12 h. (H) Representative confocal images of primary hepatocytes treated with vehicle or 10 mmol/L APAP for 12 h. Scar bar, 10 μm. Experiments A–E were performed on mice treated with saline, or 300 mg/kg APAP for 6, 12 or 24 h, or 600 mg/kg APAP for 24 h; n = 6–9 per group. Data are presented as the mean ± SEM; $*P < 0.05$.
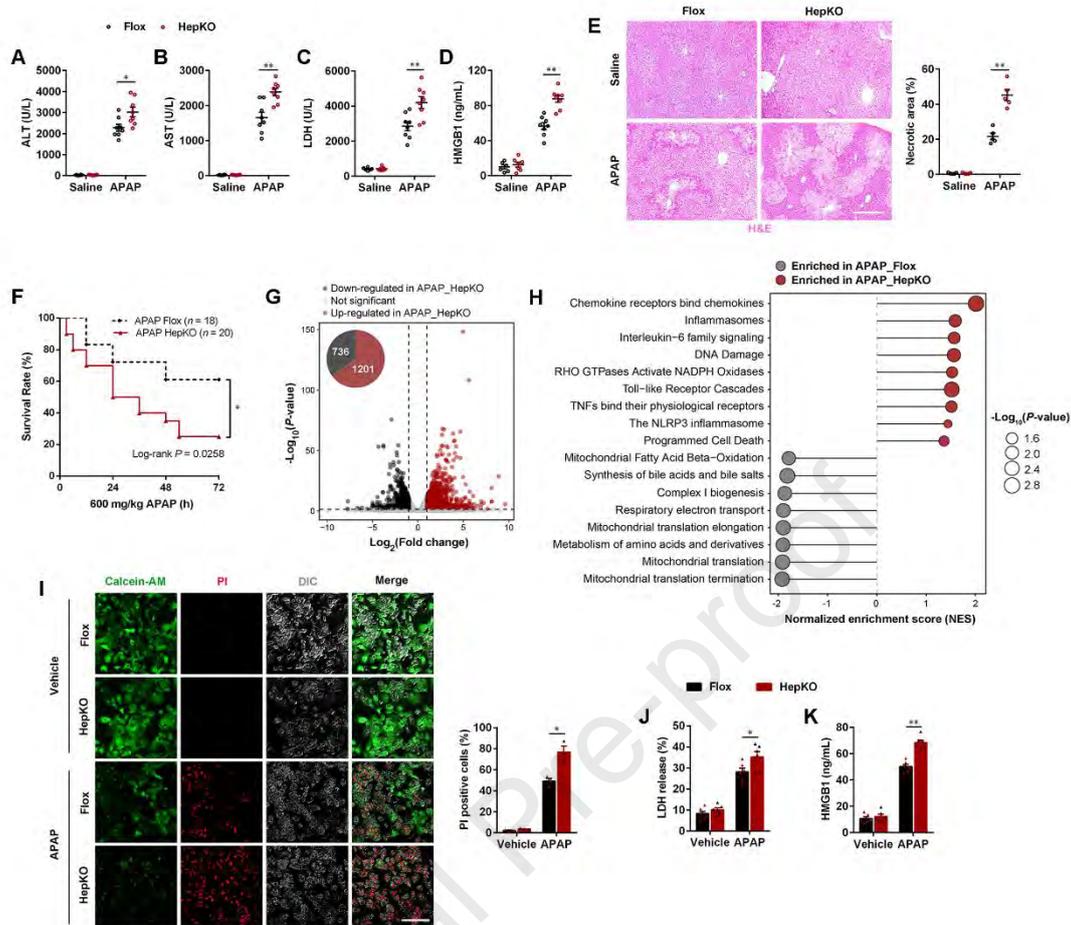
Figure 2 Hepatocyte-specific deficiency of NEDD4-1 exacerbates APAP induced hepatotoxicity *in vivo* and *in vitro*. (A–D) Serum ALT (A), AST (B), LDH (C) activities, and HMGB1 levels (D) of mice. (E) Representative H&E-stained images (left) and necrotic area quantification (right) of mouse liver sections. Scale bar, 200 μm. (F) Survival rate of Flox ($n = 18$) or HepKO ($n = 20$) mice treated with 600 mg/kg APAP for 72 h. (G, H) RNA-seq was conducted on total RNA isolated from livers of Flox or HepKO mice treated with 300 mg/kg APAP for 24 h; $n = 3$ per group. Volcano plot (G) shows the differentially expressed genes (1201 genes were up-regulated and 736 genes were down-regulated in APAP-treated HepKO mice). GSEA (H) shows the gene sets that the differentially expressed genes significantly enriched. (I) Representative images (left) and quantification (right) of Calcein-AM (green) and PI (red) double-stained primary hepatocytes. Scale bar, 200 μm. (J, K) LDH release (J) and HMGB1 level (K) in the culture medium of primary hepatocytes. Experiments A–E were performed on Flox or HepKO mice treated with saline or 300 mg/kg APAP for 24 h; $n = 5$–8 per group. Experiments I–K were performed on primary hepatocytes isolated from Flox or HepKO

mice, with vehicle or APAP (10 mmol/L for 12 h) treatment. Data are presented as the mean ± SEM; *P < 0.05, **P < 0.01.
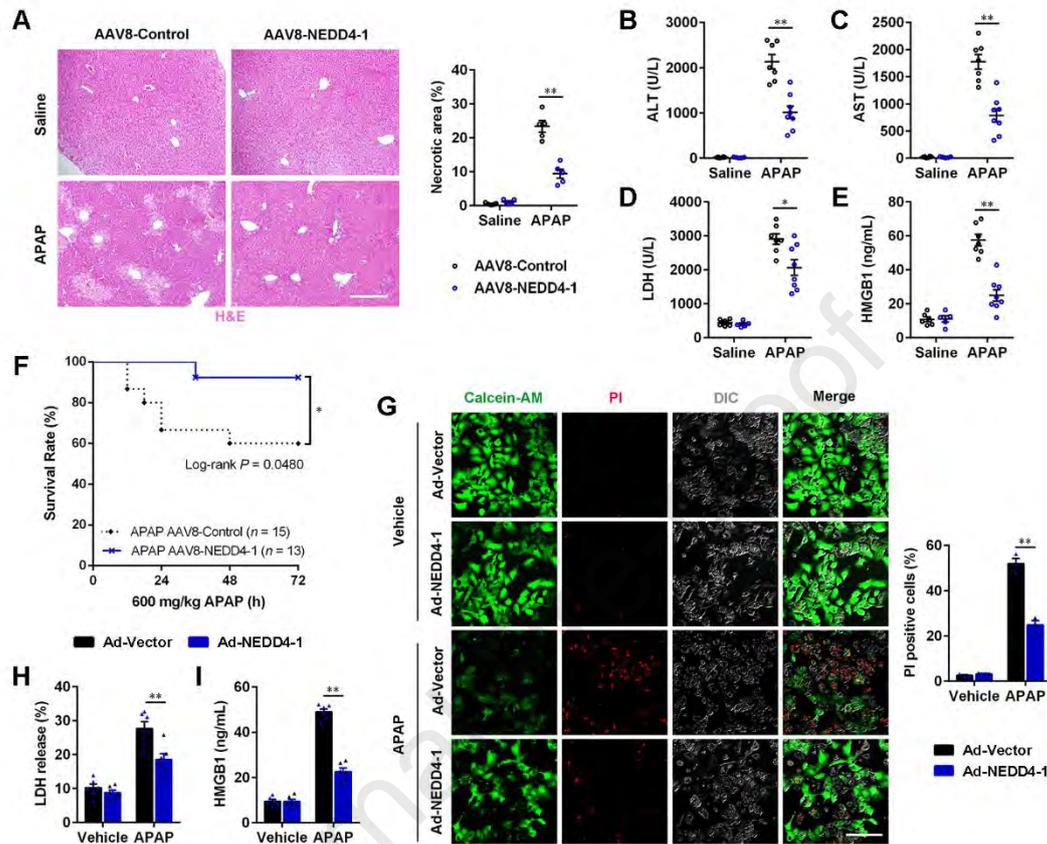
**Figure 3** Hepatocyte NEDD4-1 overexpression alleviates APAP-induced hepatotoxicity *in vivo* and *in vitro*. (A) Representative H&E-stained images (left) and necrotic area quantification (right) of mouse liver sections. Scale bar, 200 μm. (B–E) Serum ALT (B), AST (C), LDH (D) activities, and HMGB1 level (E) of mice. (F) Survival rate of AAV8-Control (n = 15) or AAV8-NEDD4-1 (n = 13) infected mice, with 600 mg/kg APAP treated for 72 h. (G) Representative images (left) and quantification (right) of Calcein-AM (green) and PI (red) double-stained primary hepatocytes. Scale bar, 200 μm. (H, I) LDH release (H) and HMGB1 level (I) in the culture medium of primary hepatocytes. Experiments A–E were performed on AAV8-Control or AAV8-NEDD4-1 infected mice, with saline or 300 mg/kg APAP treated for 24 h, n = 5–8 per group. Experiments G–I were performed on primary hepatocytes transfected with Ad-Vector or Ad-NEDD4-1, with vehicle or APAP (10 mmol/L for 12 h) treatment. Data are presented as the mean ± SEM; *P < 0.05, **P < 0.01.
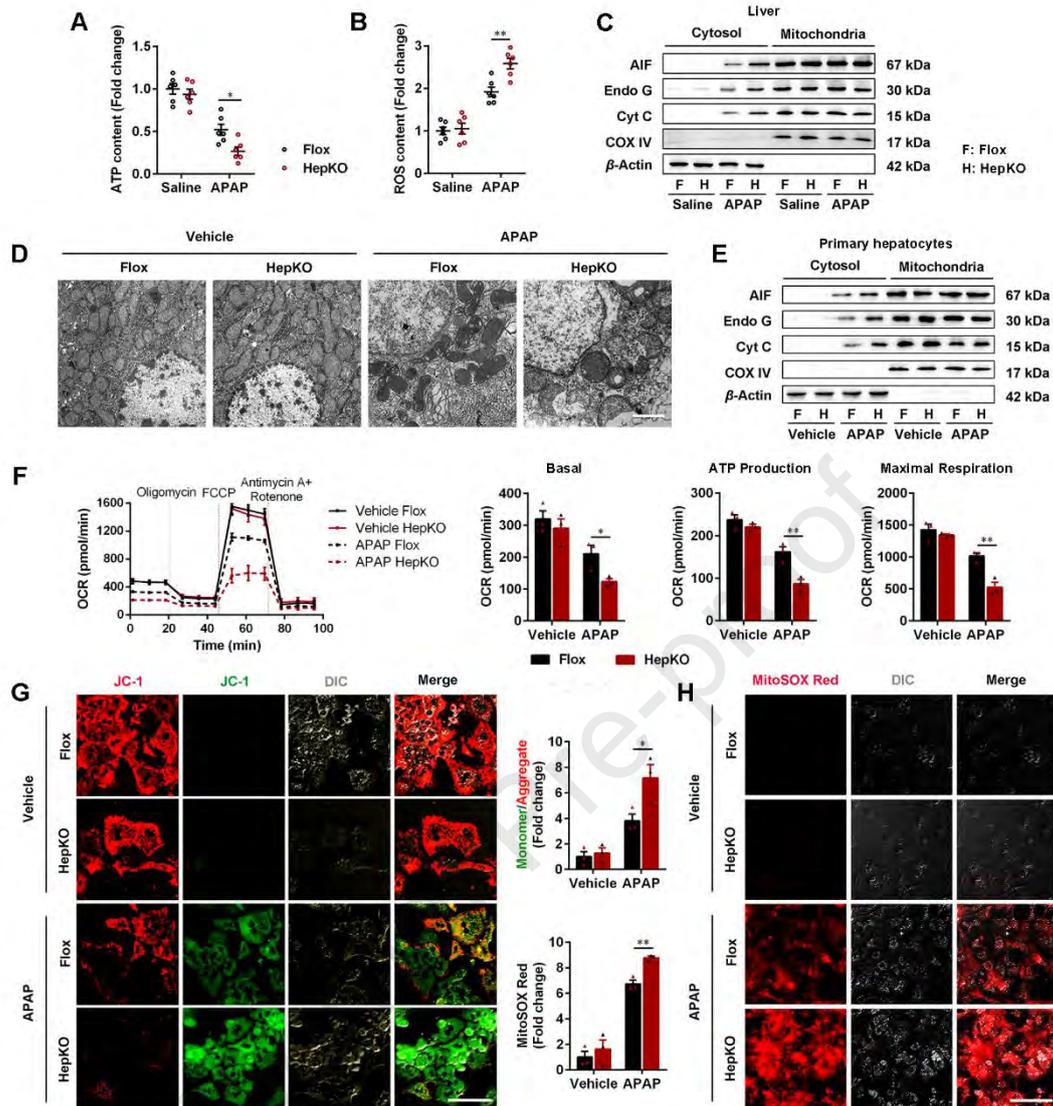
Figure 4 Hepatocyte-specific deficiency of NEDD4-1 exacerbates APAP induced mitochondrial damage *in vivo* and *in vitro*. (A, B) ATP (A) and ROS (B) contents in livers of mice. (C) Representative Western blots of indicated proteins in the cytosolic and mitochondrial fractions of liver lysates from mice. (D) Representative transmission electron microscopy micrographs of primary hepatocytes. Scale bar, 2 μm. (E) Representative Western blots of indicated proteins in the cytosolic and mitochondrial fractions of cell lysates. (F) Seahorse assays show the OCR and corresponding statistical results in primary hepatocytes. (G) Representative JC-1-stained images (left) and quantification of mitochondria depolarization (right) in primary hepatocytes. Scale bar, 100 μm. (H) Representative MitoSOX Red-stained images (right) and quantification (left) in primary hepatocytes. Scale bar, 200 μm. Experiments A–C were performed on Flox or HepKO mice treated with saline or 300 mg/kg APAP for 24 h; *n*

= 6 per group. Experiments D–H were performed on primary hepatocytes isolated from Flox or HepKO mice, with vehicle or APAP (10 mmol/L for 12 h) treatment. Data are presented as the mean ± SEM; *$P < 0.05$, **$P < 0.01$.
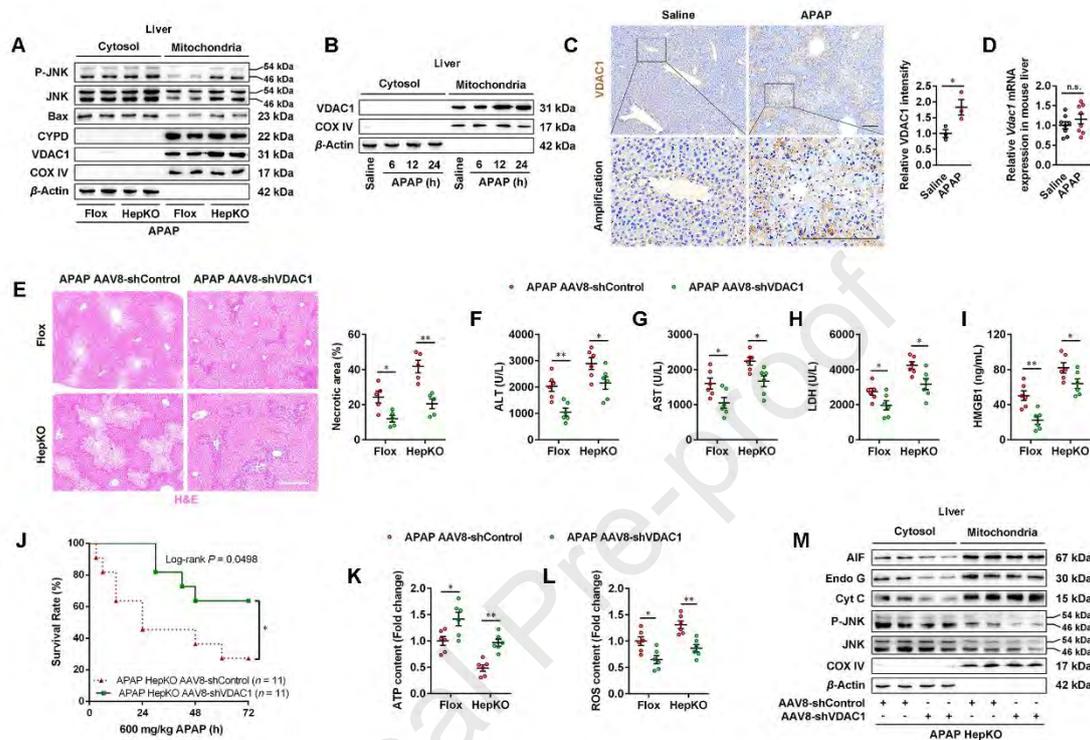
Figure 5 Knockdown of VDAC1 mitigates the enhanced AILI events caused by hepatocyte-specific NEDD4-1 deficiency *in vivo*. (A) Representative Western blots of indicated proteins in the cytosolic and mitochondrial fractions of liver lysates from Flox or HepKO mice treated with 300 mg/kg APAP for 24 h. (B) Representative Western blots of indicated proteins in the cytosolic and mitochondrial fractions of liver lysates from mice treated with saline or 300 mg/kg APAP for 6, 12 or 24 h. (C) Representative IHC staining (left) and quantification (right) in mice treated with saline or 300 mg/kg APAP for 24 h; $n = 3$ per group. Scar bar, 200 μm. (D) The hepatic mRNA expressions of *Vdac1* in mice treated with saline or 300 mg/kg APAP for 24 h; $n = 8$ per group. (E) Representative H&E-stained images (left) and necrotic area quantification (right) of mouse liver sections. Scale bar, 200 μm. (F–I) Serum ALT (F), AST (G), LDH (H) activities, and HMGB1 levels (I) of mice. (J) Survival rate of AAV8-shControl ($n = 11$) or AAV8-shVDAC1 ($n = 11$) infected HepKO mice in response to a lethal dose of APAP (600 mg/kg) for 72 h. (K, L) ATP (K) and ROS (L) contents in the livers of mice. (M) Representative Western blots of indicated proteins in the cytosolic and mitochondrial

fractions of liver lysates from AAV8-shControl or AAV8-shVDAC1 infected HepKO mice, with 300 mg/kg APAP treated for 24 h. Experiments E–I, K and L were performed on AAV8-shControl or AAV8-shVDAC1 infected Flox or HepKO mice, with 300 mg/kg APAP treated for 24 h; n = 5–6 per group. Data are presented as the mean ± SEM; *P < 0.05, **P < 0.01, n.s., not significant.
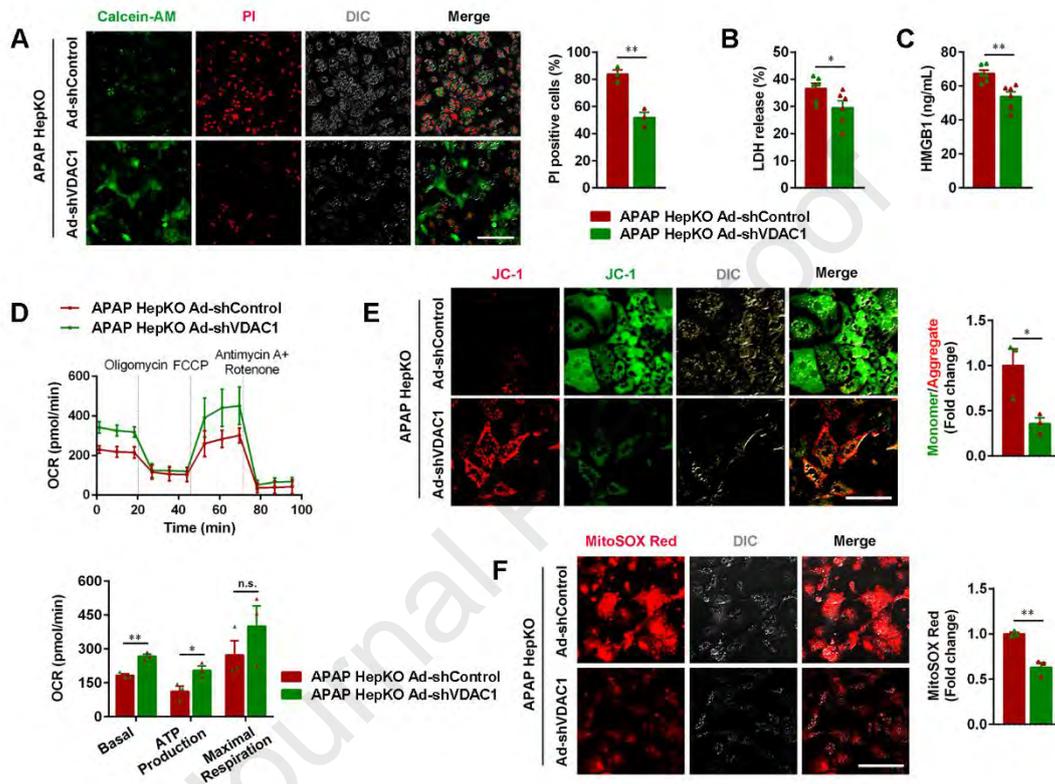

Figure 6 Knockdown of VDAC1 mitigates the enhanced APAP-induced pathological events triggered by hepatocyte-specific NEDD4-1 deficiency *in vitro*. (A) Representative images (left) and quantification (right) of Calcein-AM (green) and PI (red) double-stained primary hepatocytes. Scale bar, 200 μm. (B, C) LDH release (B) and HMGB1 level (C) in the cell culture medium. (D) Seahorse assays showed the OCR (top) and corresponding statistical results (bottom) in primary hepatocytes. (E) Representative JC-1-stained images (left) and quantification of mitochondria depolarization (right) in primary hepatocytes. Scale bar, 100 μm. (F) Representative MitoSOX Red-stained images (left) and quantification (right) in primary hepatocytes. Scale bar, 200 μm. Experiments A–F were performed on HepKO hepatocytes transfected with Ad-shControl or Ad-shVDAC1, with 10 mmol/L APAP treated for 12 h. Data are presented as the mean ± SEM; *P < 0.05, **P < 0.01, n.s., not significant.
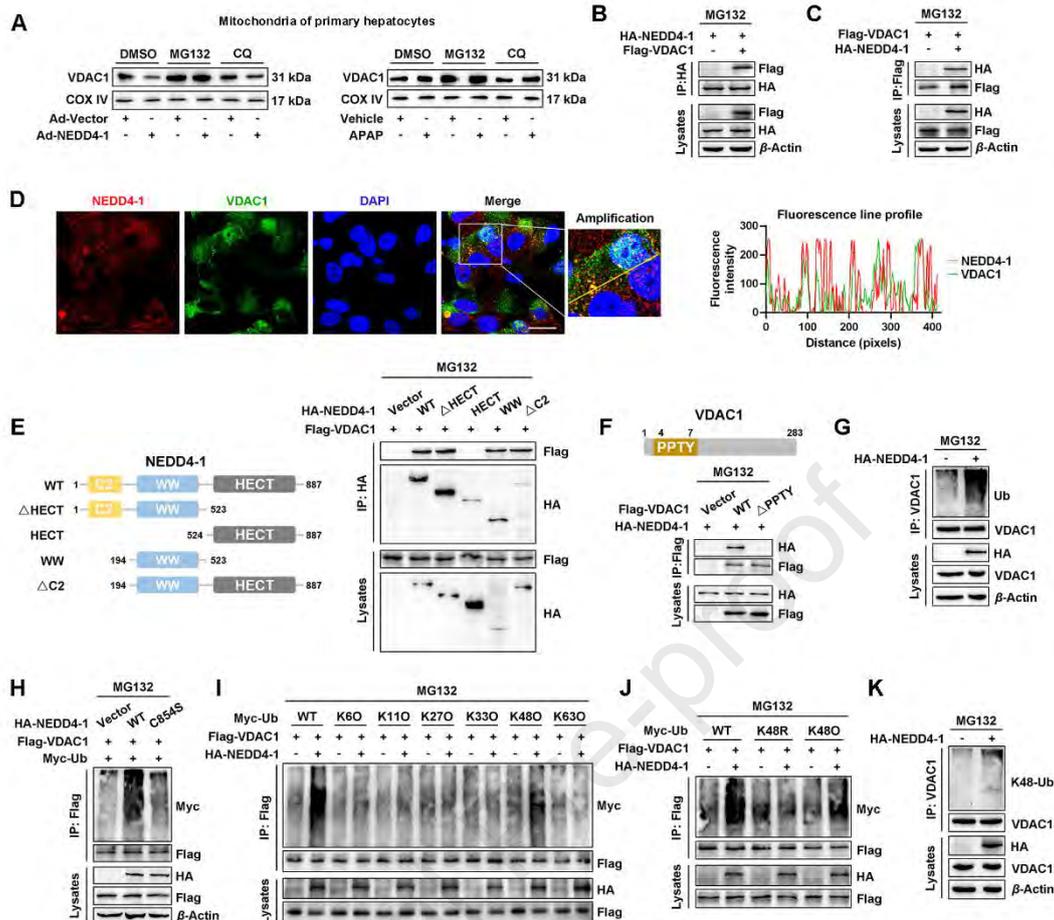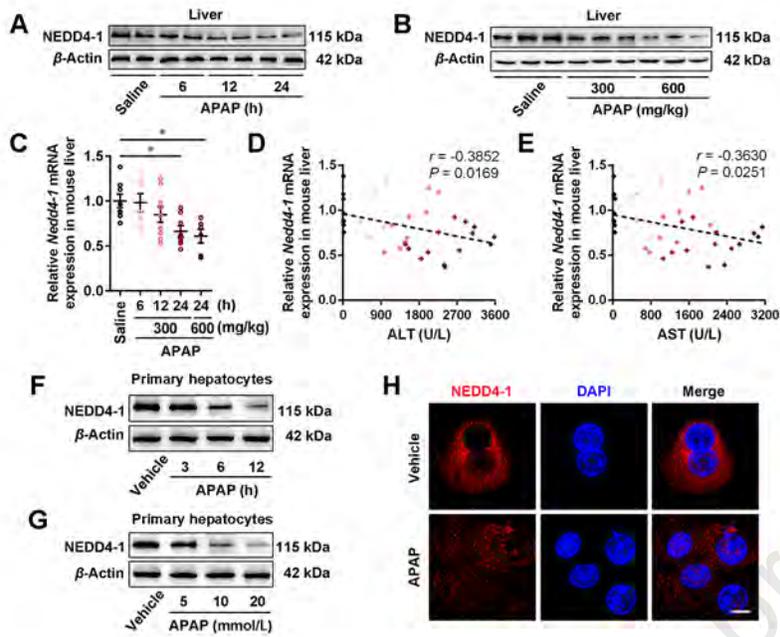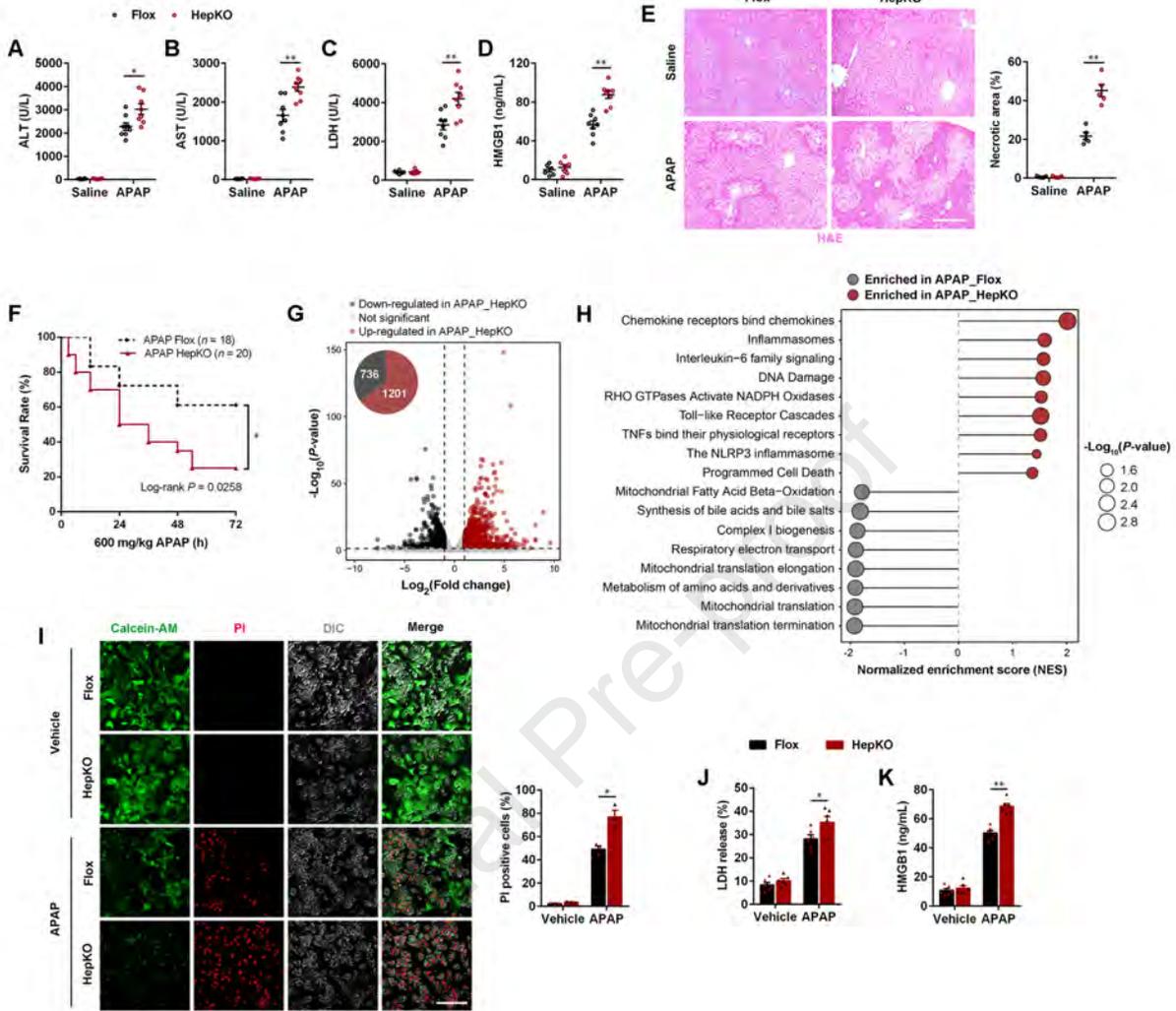
Figure 7 VDAC1 is a ubiquitination substrate of NEDD4-1. (A) Representative Western blots of indicated proteins in the mitochondrial fractions of primary hepatocytes transfected with Ad-Vector or Ad-NEDD4-1 (left) or treated with vehicle or 10 mmol/L APAP for 12 h (right**)**, with DMSO or MG132 or CQ treatment. (B, C) Representative Western blots of indicated proteins after IP with anti-HA affinity gel (B) or anti-Flag affinity gel (C), and Western blots of indicated proteins in the cell lysates of 293T cells transfected the indicated plasmids, with MG132 treatment. (D) Representative confocal images (left) and fluorescence line profile (right) of primary hepatocytes stained with NEDD4-1 (red), VDAC1 (green), and DAPI (blue). Scale bar, 30 μm. (E) Schematic (left) of mouse WT and various truncated forms of NEDD4-1 and representative Western blots (right) for Co-IP analyses in 293T cells transfected with the indicated plasmids, with MG132 treatment. (F) Schematic (top) of mouse VDAC1 and representative Western blots (bottom) for Co-IP analyses in 293T cells transfected with the indicated plasmids, with MG132 treatment. (G) Representative Western blots of ubiquitinated or total VDAC1 protein after IP with anti-VDAC1 antibody, and Western blots of indicated proteins in the cell lysates of 293T cells
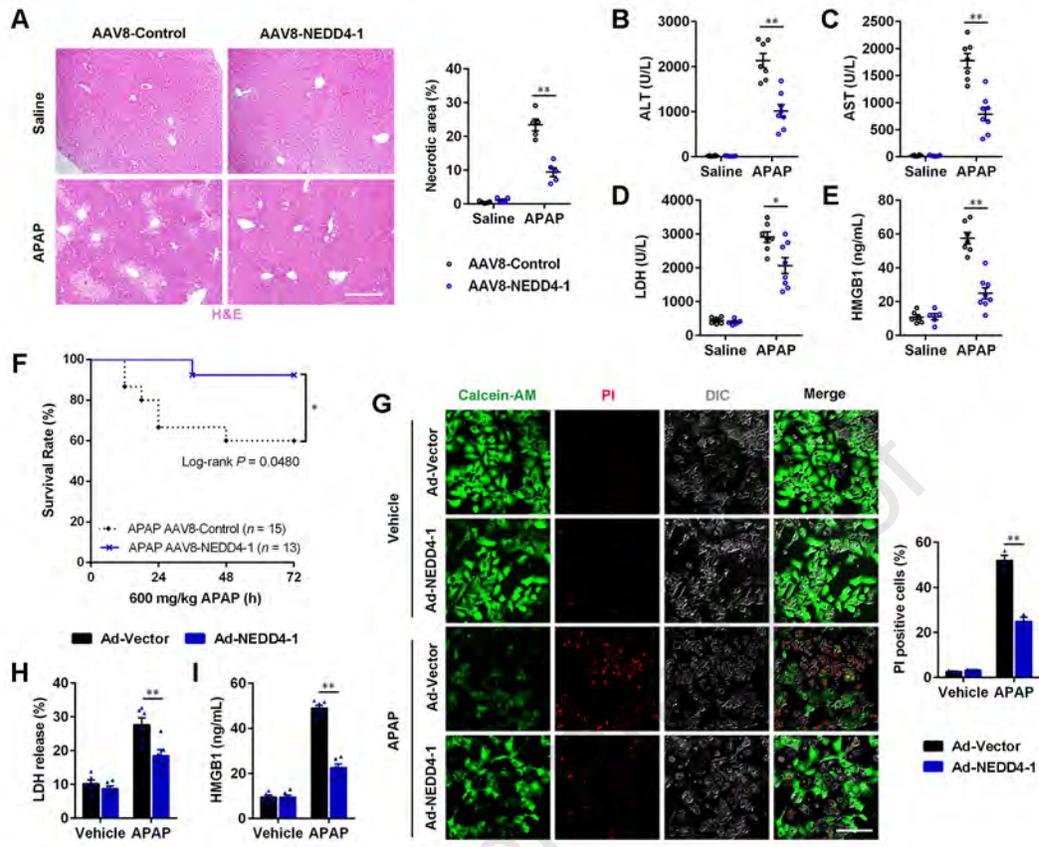
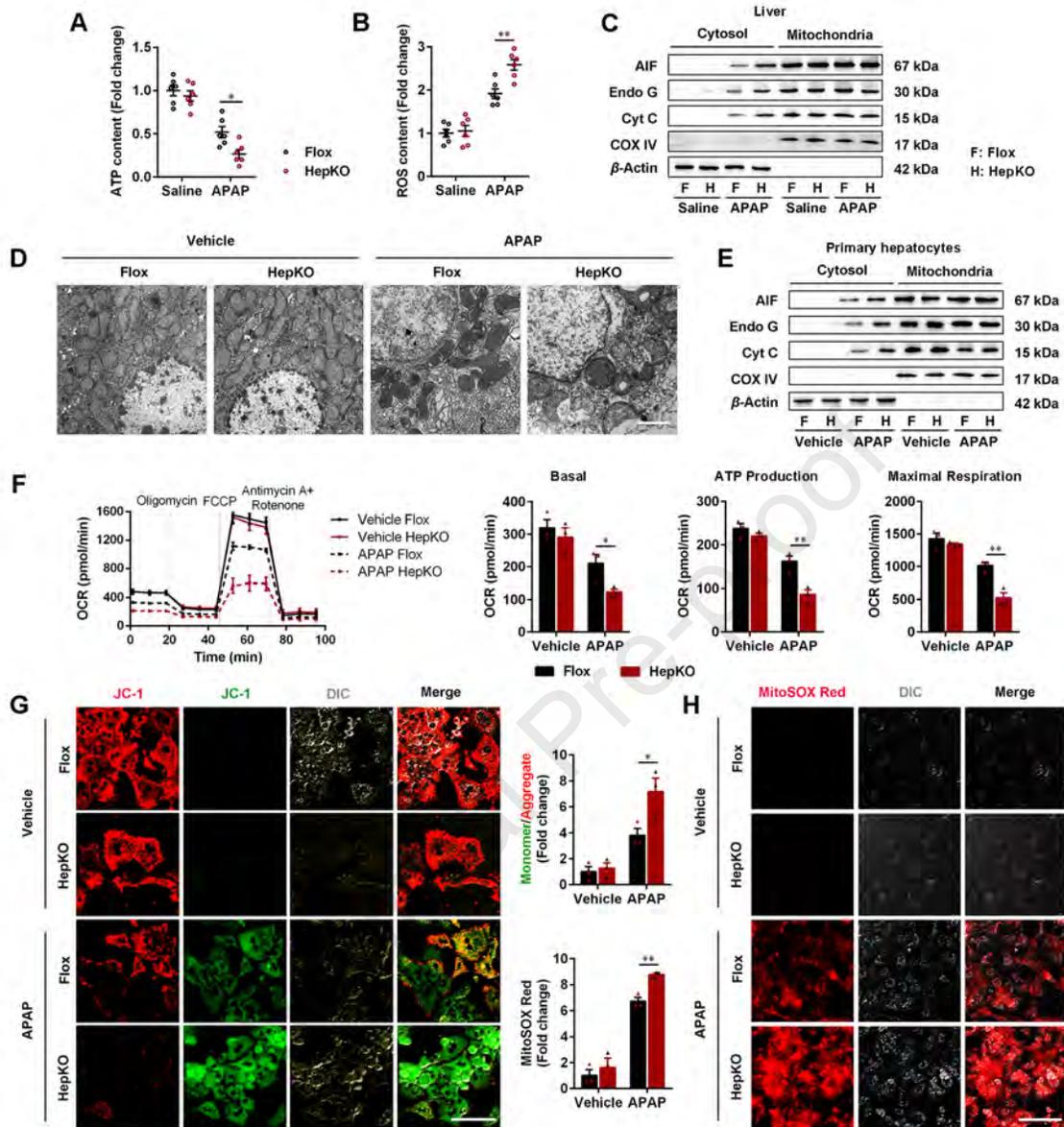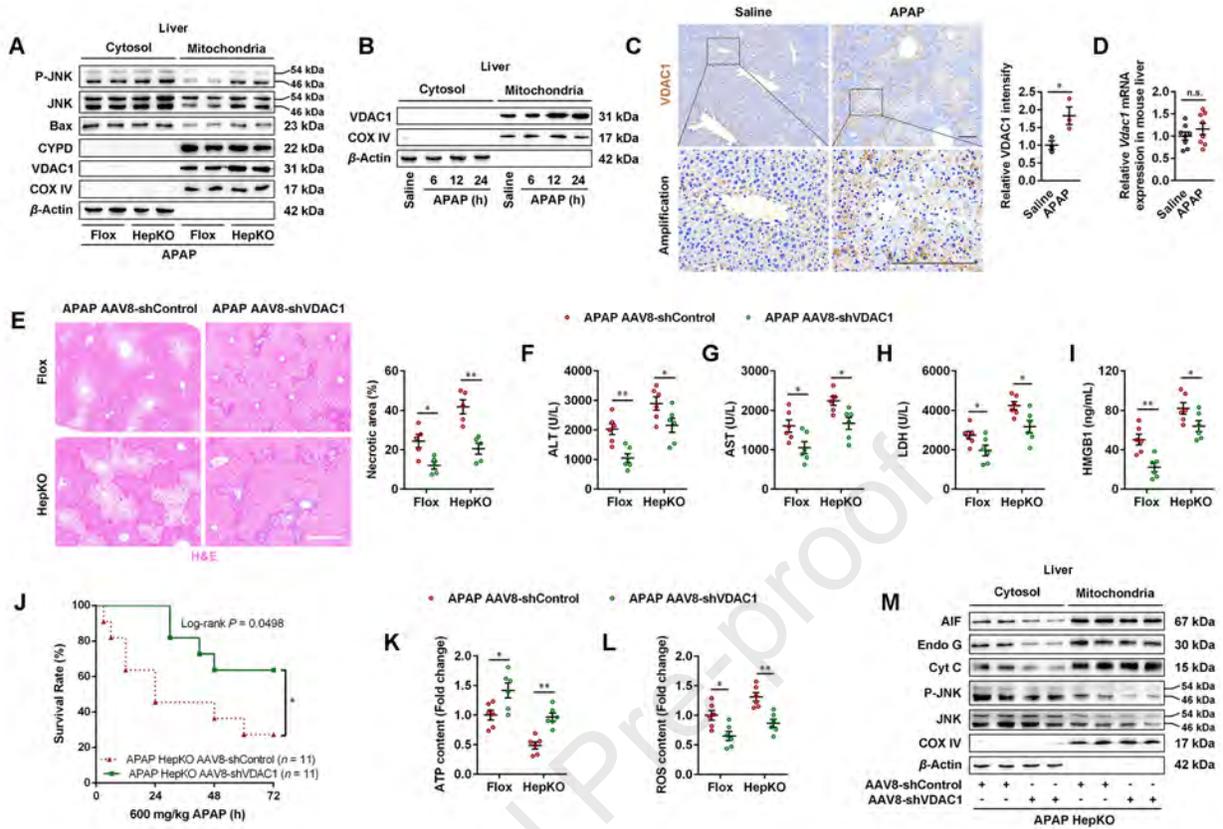transfected the indicated plasmids, with MG132 treatment. (H–J) Representative Western blots of indicated proteins after IP with anti-Flag affinity gel, and Western blots of indicated proteins in the cell lysates of 293T cells transfected the indicated plasmids, with MG132 treatment. (K) Representative Western blots of K48-Ub-linkaged or total VDAC1 protein after IP with anti-VDAC1 antibody, and Western blots of indicated proteins in the cell lysates of 293T cells transfected the indicated plasmids, with MG132 treatment.
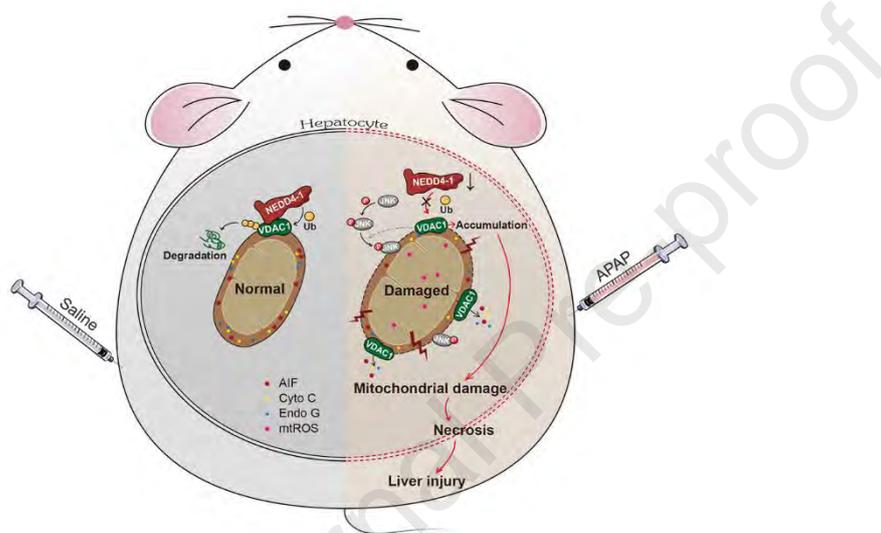
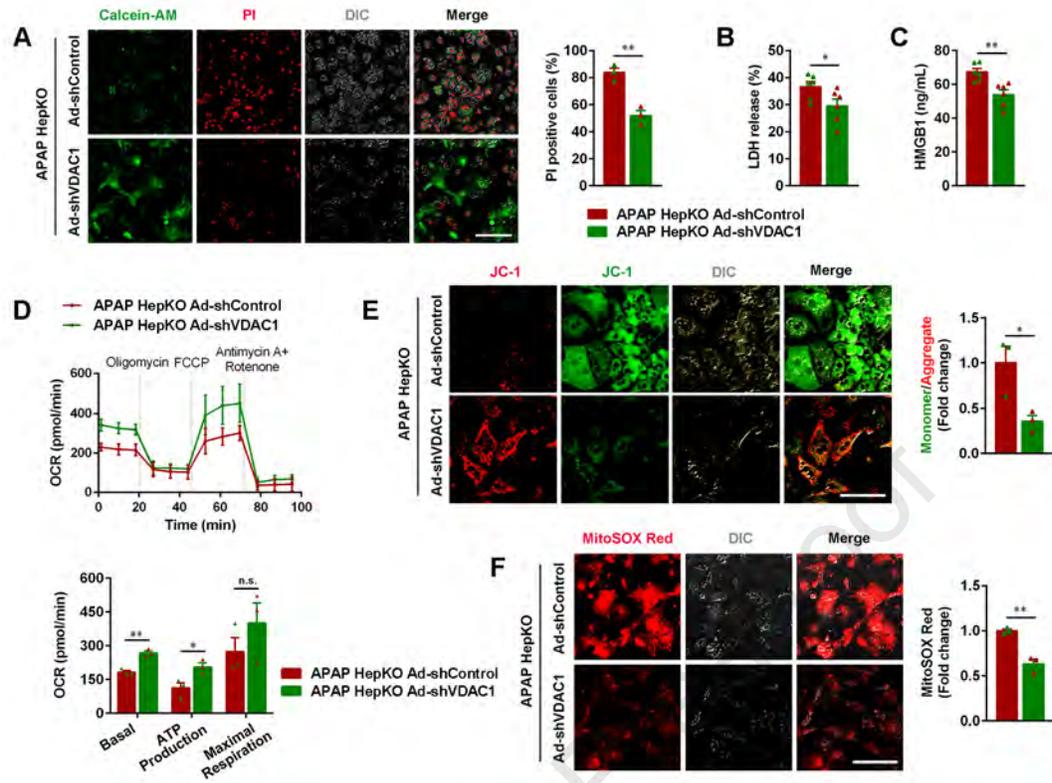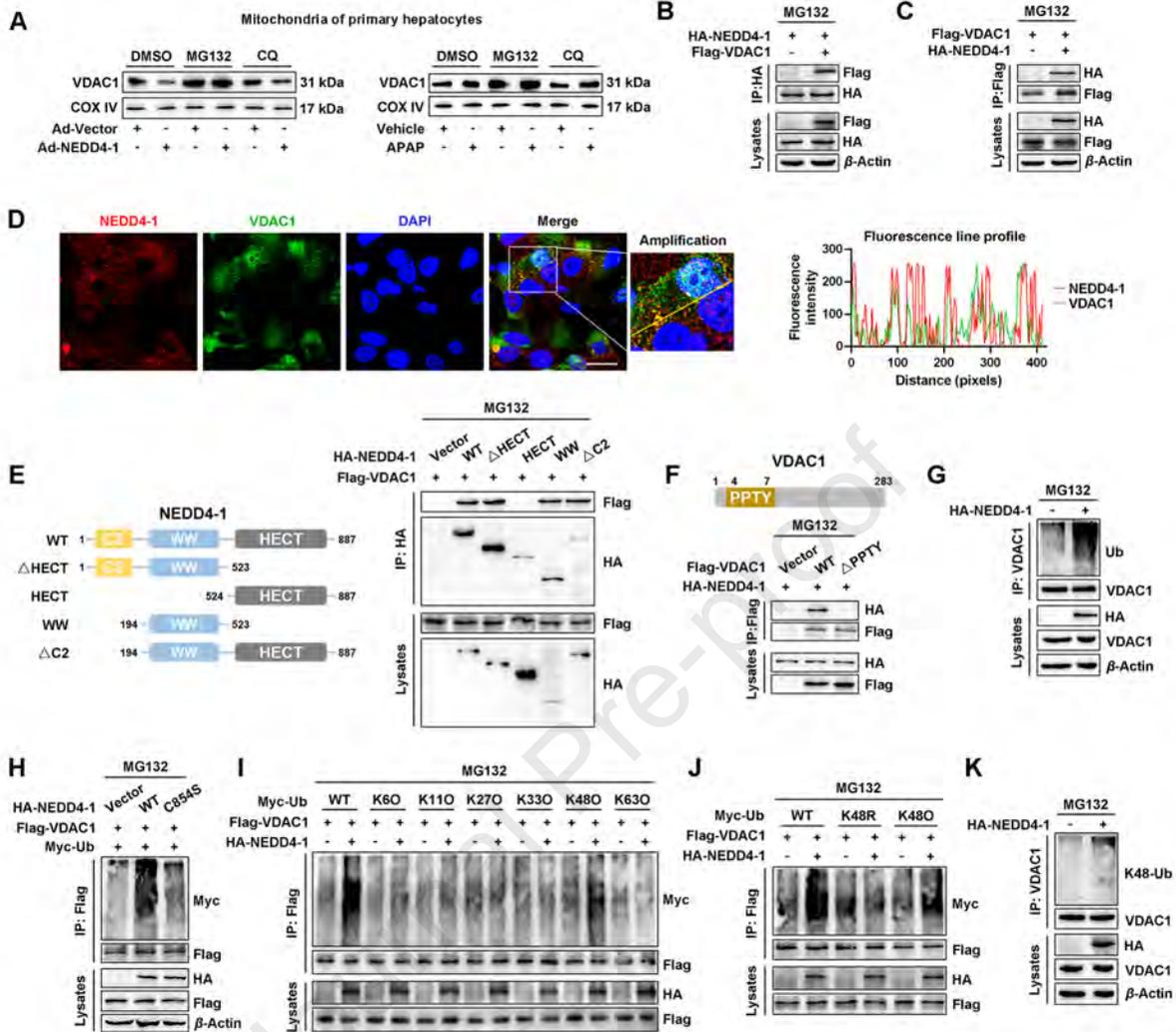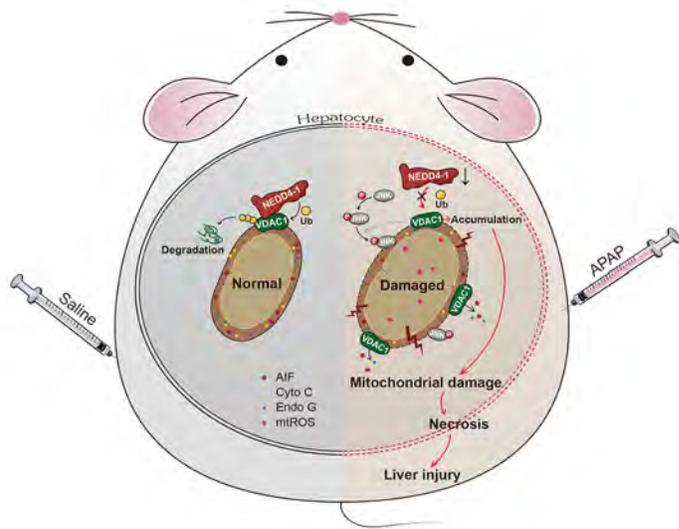**Figure 8** Schematic representation modeling that the E3 ubiquitin ligase NEDD4-1 suppresses AILI in mouse by targeting VDAC1 for degradation.